

# Numerical Schemes for problems of Phase Separation

National Technical University of Athens



Thesis submitted for M.Sc. Program in Computational Mechanics

supervised by M.Kavousanakis

Chantzaras Lampros

November 23, 2023



## Acknowledgments

Firstly i would like to thank my thesis supervisor, Mihalis Kavousanakis, Assistant Professor of the School of Chemical Engineering at the National Technical University of Athens, for his insightful advice and guidance throughout the course of this thesis.

A special thanks also goes to my younger brother Giannis, for his patience and his willingness to devote serious amount of time and his specific knowledge on computer science, to help me with every implementation aspect. His effort was crucial to completing this thesis.

Finally, I want to thank all my colleagues and the Professors of this Joint Postgraduate Studies Program, for our collective interaction throughout the last two years set the cornerstones of developing my understanding on the core subjects of the program.

# Abstract

The Cahn–Hilliard (CH) equation is a mathematical model of the process of phase separation in a binary alloy [1].

Initially proposed in view of applications to metallurgy and materials science to study phase separation and coarsening in materials, such as binary alloys, polymers, and liquid crystals, also to study the growth and morphology of thin films in material deposition processes, such as epitaxial growth. These applications have been extended to various scientific fields, including spinodal decomposition in the context of statistical mechanics, where it is used to describe the process in which a homogeneous mixture separates into two distinct phases [1, 2], diblock copolymer, image inpainting, multiphase fluid flows where it can be used to model the behavior of two immiscible fluids, like oil and water, and their interface dynamics, amongst others [3], microstructures with elastic inhomogeneity [4], tumor growth simulation [5], and topology optimization [6].

In the Cahn-Hilliard equation, the evolution of concentration consists of two stages: Fast phase separation where the energy decay happens quickly, i.e. on a small time scale, is followed by phase coarsening until the two different phases obtain constant curvature. Fine-scaled phase regions separated by the interface form at the end of the first stage, while the solution reaches an equilibrium state minimizing the energy functional at the end of the second stage.

Numerical methods that are developed for the Cahn-Hilliard equation often should take into account the nonlinearity in the system, the presence of the small parameter  $\epsilon$  (thickness of the interface), and the different time scales that characterise the concentration evolution. Resolution schemes require proper scaling of numerical parameters, such as the spatial mesh size  $h$  and often adaptive time stepping techniques for the time step size  $k$ , relative to the interaction length  $\epsilon$ .

The aim of this thesis, is to present a range of the main numerical methods that have been applied to the mixed finite element approximation of the solution to the Cahn-Hilliard equation problems. These numerical schemes offer different orders of accuracy in time and vary also regarding their numerical stability and the solvability of the time discrete equations that arise. Fundamental ideas like the convex splitting are also illustrated, as their significance and versatility has become central in the study of numerical schemes for the Cahn Hilliard equation.

The implementation that has been developed for this work illustrates the effectiveness and the high accuracy of the common Backward Euler numerical scheme arising from the standard conforming mixed finite element formulation of this problem. For the approximation in space we employ the biquadratic shape functions that are defined on the standard 9-node Lagrange quadrilateral reference element. The resulting nonlinear algebraic system for every time step is then solved by a Newton-Raphson iteration procedure and during each iteration, a linear system with the corresponding Jacobian has to be solved. For this linear system the biconjugate gradient method (BiCGStab) method is employed. Two main cases for the boundary conditions to close the problem are examined. The first is the periodic in one or two directions and the second refers to the specified contact angle of the phase field with the boundary. The last chapter is concerned with certain optimization directions that would allow for higher degrees of freedom approximations, thus a more realistic simulation of the phase transition phenomena that occur.

# Contents

<b>1</b>	<b>Introduction</b>	<b>7</b>
1.1	The basic framework of the Phase Field Model . . . . .	7
1.2	Statement of the problem . . . . .	10
1.3	The weak formulation . . . . .	11
1.4	The finite element discretization . . . . .	12
1.5	The semi-discrete approximation . . . . .	13
1.6	The fully discretized problem . . . . .	14
<b>2</b>	<b>The temporal discretization</b>	<b>15</b>
2.1	First-order accurate schemes . . . . .	16
2.1.1	Backward Euler . . . . .	16
2.1.2	First-order semi-implicit method . . . . .	17
2.1.3	Convex-Splitting Method . . . . .	17
2.2	Stability and Solvability Analysis for Second-order Schemes . . . . .	18
2.2.1	Crank–Nicolson Method . . . . .	18
2.2.2	Second-order Semi-implicit Method . . . . .	19
2.2.3	Secant Method . . . . .	19
2.2.4	Second-order Convex Splitting . . . . .	20
2.3	Stabilization . . . . .	20
<b>3</b>	<b>The Newton-Raphson procedure</b>	<b>22</b>
<b>4</b>	<b>The periodic problem</b>	<b>24</b>
4.1	Statement of the problem . . . . .	24
4.2	The finite dimensional projection of the solution . . . . .	24
4.3	The system’s matrices . . . . .	27
4.4	The nonlinear term . . . . .	28
4.5	The boundary flux matrix . . . . .	29
4.6	The algorithm for the periodic problem . . . . .	30
4.6.1	Experiments-Results . . . . .	32
<b>5</b>	<b>Phase-field model for wetting phenomena</b>	<b>34</b>
5.1	Statement of the problem . . . . .	34
5.2	The weak formulation . . . . .	35
5.3	The temporal discretization and the algorithm . . . . .	35
5.3.1	Experiments-Results . . . . .	36
<b>6</b>	<b>Conclusions and future directions for the development of the code</b>	<b>39</b>
6.0.1	Adaptive time stepping . . . . .	39
6.0.2	Broyden’s Method . . . . .	40
<b>A</b>	<b>The implementation</b>	<b>44</b>
A.1	Dependencies . . . . .	44
A.2	Program Components . . . . .	44
A.3	Space and Time Coordinates . . . . .	44
A.4	Local to Global Node Numbering . . . . .	44
A.5	Order Parameter Variables . . . . .	44
A.6	Chemical Potential Variables . . . . .	44
A.7	Newton Tolerance Parameters . . . . .	44
A.8	Stationary System of Newton Cycle . . . . .	45
A.9	Local Contributions . . . . .	45
A.10	Newton Solution Vector . . . . .	45
A.11	Loop Variables . . . . .	45

A.12 Convergence Check . . . . .	45
A.13 File Handling . . . . .	45
A.14 Program Execution . . . . .	45
A.15 Space Discretization . . . . .	46
A.16 Global Node Numbering . . . . .	46
A.17 Time Discretization . . . . .	47
A.18 Initial Conditions . . . . .	47
A.19 The system of each Newton cycle . . . . .	48
A.20 The test functions . . . . .	51
<b>B PERIODIC.f90</b>	<b>52</b>
<b>C CONTACTANGLE.f90</b>	<b>56</b>

# 1 Introduction

The most attractive feature of the Cahn Hilliard equation is that it is used to describe a wide variety of phenomena that exhibit phase transition ranging from nanoscale precipitation to the forming of galaxies in the universe [7]. So the necessity to develop numerical schemes is interconnected with extracting valuable information about the behavior of the solution that can be used to verify the theoretical considerations about the evolution of phase transition processes and also can contribute to the development of a wide range of industrial applications. The forementioned considerations constitute the author's motives to study the subject.

## 1.1 The basic framework of the Phase Field Model

In this chapter we present the essential considerations for the derivation of the phase field model for the sake of completeness of the work to follow. For the interested reader the rigorous derivation of the phase-field model can be found to: [8]. Also an instructive review of the main ways to derive the Cahn-Hilliard equation can be found in [9].

The standard approach is to consider a binary fluid system consisting of two immiscible viscous fluids, denoted as fluids 1 and 2 under constant temperature, completely occupying a bounded domain  $\Omega$  in  $\mathbb{R}^2$  (for our work), with a sufficiently smooth boundary denoted as  $\partial\Omega$ . The total density of the mixture is defined as  $\rho_m = \frac{m}{V}$  is considered constant,  $m$  represents the total mass of the mixture in the volume of the system  $V$  (i.e.,  $m = \int_{\Omega} \rho_m dV$ ). We assume that the two fluids possess different apparent densities defined as  $\rho'_i = \frac{m_i}{V}$  also constants for  $i = 1, 2$ . We define the apparent densities as  $\rho'_i$ . These are related to the actual densities  $\rho_i = \frac{m_i}{V_i}$  through  $\rho'_i = V_{f_i} \rho_i$ , where  $V_{f_i} = \frac{V_i}{V}$  represent the volume fractions, and  $m_i$  represents the masses of the components in  $\Omega$ , defined as:

$$m_i = \int_{\Omega} \rho'_i dV,$$

The total mass  $m$  is the sum of the masses of fluids 1 and 2:

$$\rho_m = \rho'_1 + \rho'_2$$

The interface between the two phases has a thin nonzero thickness characterized by a rapid and smooth transition. The scalar function  $\phi$ , known as the "order parameter" is used to represent the two phases and the transition in between.

$$\phi = \begin{cases} 1, & \text{in fluid 1,} \\ -1, & \text{in fluid 2,} \\ [-1, 1], & \text{in the interfacial region.} \end{cases}$$

The origin of the spatial transition between the two materials is considered to be the local surface tension (we assume constant temperature, incompressibility of the fluids and viscosity). Consequently, the total amount of each fluid in  $\Omega$  must remain constant and the principles of mass conservation and of the linear momentum of continuum mechanics apply.

The function  $\phi$  can be thought of as the difference in local mass fraction of the two fluids:

$$\phi = \frac{\rho'_1 - \rho'_2}{\rho'_1 + \rho'_2},$$

or equivalently,

$$\phi dm_i = \rho'_1 dm_i dV - \rho'_2 dm_i dV$$

By further manipulation, we obtain

$$\phi \rho_m = \rho'_1 \rho'_2$$

We observe that  $\phi \in [-1, 1]$ . When  $\phi = 1$  or  $\phi = -1$ , only fluid 1 or 2 exists, respectively. Moreover, recalling the definitions of  $\rho'_1$  and  $\rho'_2$ , we find that

$$\int_{\Omega} \rho_m \phi dV = \left( \int_{\Omega} \rho'_1 dV \right) \left( \int_{\Omega} \rho'_2 dV \right) = m_1 m_2 = \text{constant}.$$

This demonstrates that the definition of  $\phi$  ensures the conservation of the concentration difference between the two fluids in  $\Omega$ . The conservation of the mass of each component across the entire domain imposes the constraint:

$$\int_{\Omega} \rho_m \phi(x, t) dV = \text{constant}$$

The relaxation of the order parameter is driven by local minimization of the free energy subject to phase field conservation and as a result, the interface layers do not deteriorate dynamically. The width of the interfacial layer depends on a parameter  $\epsilon$  appearing in the system, and as  $\epsilon$  tends to zero, the diffuse interface system converges to the corresponding sharp interface one. Initial ideas can be traced back to van der Waals and form the foundation for the phase-field theory, for phase transition and critical phenomena. The phase field motion is governed by a bulk field over the entire domain, and it inherits various interesting properties, including the coupling with physical variables (e.g., velocity and pressure in fluids, temperature), through the combined models with the Navier Stokes equations.

For our setting we consider the energy functional  $E_{\epsilon}(\phi)$  to represent different interfacial energies associated with the phase field, given by (1):

$$E_{\epsilon}(\phi) = \int_{\Omega} \left( \frac{1}{2} |\nabla \phi|^2 + \frac{1}{\epsilon^2} W(\phi) \right) dV \quad (1)$$

where  $W(\phi)$  is a double-well potential (typically expressed in the form of (2)), representing the system's tendency to have two different stable phases, and  $\epsilon > 0$  is the parameter related to the interface thickness. Figure 1 describes the typical form of the double well potential.

$$W(\phi) = \frac{1}{4} (\phi^2 - 1)^2 \quad \text{and} \quad f(\phi) = W'(\phi) = (\phi^2 - 1)\phi. \quad (2)$$

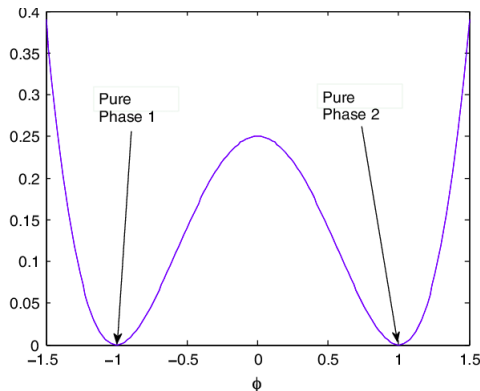


**Figure 1:** The typical form for the potential



There are other possible choices for the double well potential, such as the logarithmic potential, but we concentrate on the Ginzburg-Landau polynomial type potentials in this work.

The surface motion can be derived as the dissipation of a phase-field's free energy functional. Here  $\frac{\delta E(\phi)}{\delta \phi}$  in (3), represents the variational derivative in the  $L^2(\Omega)$  or  $H^{-1}(\Omega)$  norm for the Cahn-Hilliard equation.

$$\frac{\delta E(\phi)}{\delta \phi} = \int_{\Omega} \left( -\Delta \phi + \frac{1}{\epsilon^2} W'(\phi) \right) dx \quad (3)$$

Under the above considerations one can derive the solution of the Cahn-Hilliard equation as minimization of the energy functional under the constraint of the constant mean concentration.

## 1.2 Statement of the problem

Under the laws of thermodynamics we need to ensure that the total "free energy" of the mixture decreases over time. For this purpose, we consider that the mixture cannot pass through the boundary of the domain. This means that the outward normal derivatives of  $\phi$  and  $\Delta\phi - f(\phi)$  must vanish on  $\partial\Omega$ .

Using the mass balance law:

$$\frac{\partial\phi}{\partial t} + \gamma\nabla \cdot \mathbf{J} = 0, \quad (4)$$

In (4) the introduced  $\gamma > 0$  often denotes a relaxation time constant and  $\mathbf{J}$  is the phase flux defined as:

$$\mathbf{J} = -M(\phi)\nabla \left( \frac{\partial E(\phi)}{\partial\phi} \right), \quad (5)$$

$M(\phi)$  represents the mobility function.

For simplicity purposes and to illustrate the main ideas without unnecessary manipulations, we consider a constant value for the mobility,  $M(\phi) = 1$ .

Under these assumptions, the Cahn-Hilliard problem can be expressed as:

$$\frac{\partial\phi}{\partial t} = \gamma\nabla \cdot \left( \nabla \left( -\nabla^2\phi + \frac{1}{\epsilon^2}W'(\phi) \right) \right) \text{ in } \Omega \times (0, T), \quad (6)$$

$$\frac{\partial\phi}{\partial n} = 0, \quad \frac{\partial}{\partial n} \left( -\nabla^2\phi + \frac{1}{\epsilon^2}W'(\phi) \right) = 0 \text{ on } \partial\Omega \times (0, T), \quad (7)$$

$$\phi|_{t=0} = \phi_0 \text{ in } \Omega. \quad (8)$$

For this work we replace the zero flux conditions with the more general contact angle conditions that are stated in a separate chapter, as well as with the periodic conditions, in an effort to capture repeatedly occurring patterns often encountered in materials modeling applications.

### 1.3 The weak formulation

Formally, the Cahn-Hilliard equation is a fourth-order, nonlinear parabolic partial differential equation. A convenient way to handle the fourth order derivative is to rewrite the problem using the chemical potential  $\mu$  as an auxiliary unknown:

$$\frac{\partial \phi}{\partial t} = \gamma \nabla \cdot \nabla \mu, \quad (9)$$

$$\mu = -\nabla^2 \phi + \frac{1}{\epsilon^2} W'(\phi) \text{ in } \Omega \times (0, T), \quad (10)$$

$$(11)$$

This manipulation is more than just a trick. It is an essential idea that enables the use of lower degree polynomials to approximate the solution on the discretized element domain.

The weak formulation of this problem can be defined as follows: Find  $(\psi, \eta)$  such that  $\psi \in L^\infty(0, T; H^1(\Omega))$ ,  $\phi_t \in L^2(0, T; (H^1(\Omega))')$ , and  $\eta \in L^2(0, T; H^1(\Omega))$  satisfying the following variational formulation:

$$\int_{\Omega} \mu \eta \, dx + \int_{\partial\Omega} \eta (\nabla \phi \cdot n) \, ds - \int_{\Omega} \nabla \phi \cdot \nabla \eta \, dx - \frac{1}{\epsilon^2} \int_{\Omega} W'(\phi) \eta = 0 \quad (12)$$

$$\int_{\Omega} \frac{\partial \phi}{\partial t} \psi \, dx - \int_{\partial\Omega} \psi (\nabla \mu \cdot n) \, ds + \gamma \int_{\Omega} \nabla \mu \cdot \nabla \psi \, dx = 0 \quad (13)$$

where  $n$  denotes the surface normal vector.

On a more compact notation we may use,  $(f, g) := \int_{\Omega} f(x)g(x)dx$  to represent the standard product in the  $L^2(\Omega)$  space, and  $\langle \phi_t, \psi \rangle$  for the dual space product between  $(H^1(\Omega))'$  and  $H^1(\Omega)$ , respectively.

The total mass is conserved in time, i.e.,  $\int_{\Omega} \phi(t)$  remains constant in time, which can be realized by testing with  $\psi = 1$  in the weak formulation:

$$\frac{d}{dt} \int_{\Omega} \phi = 0, \quad \text{i.e.,} \quad \int_{\Omega} \phi(t) = \int_{\Omega} \phi_0, \quad \forall t \geq 0 \quad (14)$$

## 1.4 The finite element discretization

We consider our domain to be a rectangle in two dimensions and we opt for a subdivision of  $\Omega$  into non-overlapping rectangles such that no vertex of any rectangle lies on a side of another rectangle. We consider 9 nodal points on each element, as shown in Figure 2:

Let  $Q_2(\Omega)$  be the set of biquadratic functions on  $K$ , i.e.,

$$Q_2(\Omega) = \left\{ v : v(x) = \sum_{i=0}^2 a_{ij} x^i y^j, \text{ for } x, y \in \Omega, \text{ where } a_{ij} \in \mathbb{R} \right\}$$

which can be thought as the product of the corresponding one dimensional quadratic functions on  $x, y$ . The shape functions defined under the constraint to be 1 on the node they refer to and zero on every other node of the element, that are used for the approximation on the reference element are depicted in Figure 3.

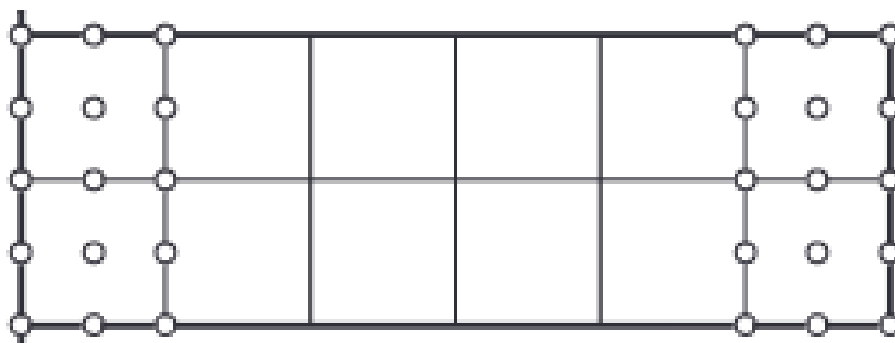


**Figure 2:** The domain decomposition on 9-node elements

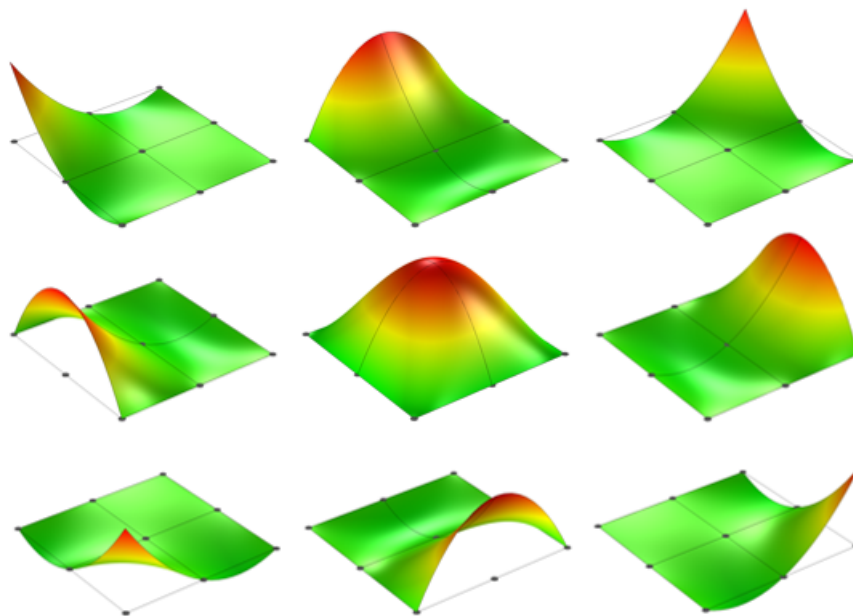


**Figure 3:** The shape functions on the 9-node reference element

## 1.5 The semi-discrete approximation

Next, consider  $h$  to represent the spacing of the nodes on a uniform configuration of a certain number of elements, as shown in Figure 2 above. We compute the finite element approximation  $\mu_h$  and  $\phi_h$ , considering  $\{\psi_i\}_{i=1}^N$  to be the biquadratic Lagrange polynomial functions. We can write the solution and the chemical potential approximations as:

$$\mu_h(t) = \sum_{j=1}^N \mu_j(t) \psi_j \quad (15)$$

$$\phi_h(t) = \sum_{j=1}^N \phi_j(t) \psi_j \quad (16)$$

with  $2N$  time-dependent unknowns  $\mu_j(t)$ ,  $\phi_j(t)$  for  $j = 1, 2, \dots, N$  to be found. We therefore approximate the solution values for a fixed time. A rigorous proof to justify the good approximation properties of this approach would refer to Bochner Spaces and to the relevant theory of the analysis of PDEs, but is out of the scope of this work.

Inserting (15),(16) to (12),(13) we obtain:

$$\int_{\Omega} \sum_{j=1}^N \mu_j(t) \psi_j \psi_i dx + \int_{\partial\Omega} \psi_i (\nabla (\sum_{j=1}^N \phi_j(t) \cdot n) \cdot n) ds - \int_{\Omega} \nabla (\sum_{j=1}^N \phi_j(t) \psi_j) \cdot \nabla \psi_i dx - \frac{1}{\epsilon^2} \int_{\Omega} W'(\sum_{j=1}^N \phi_j(t) \psi_j) \psi_i = 0 \quad (17)$$

$$\int_{\Omega} \frac{\partial \sum_{j=1}^N \phi_j(t) \psi_j}{\partial t} \psi_i dx - \int_{\partial\Omega} \psi_i (\nabla (\sum_{j=1}^N \mu_j(t) \cdot n) \cdot n) ds + \gamma \int_{\Omega} \nabla (\sum_{j=1}^N \mu_j(t) \psi_j) \cdot \nabla \psi_i dx = 0 \quad (18)$$

## 1.6 The fully discretized problem

Using the fact that the nodal coefficients  $\mu_j(t)$ ,  $\phi_j(t)$  for  $j = 1, 2, \dots, N$  have only temporal dependence and since we can interchange the (finite) summation with the integral, we can deduce the form of the mass, stiffness matrices and of the boundary and the non linear term respectively, that correspond to the fully discretized version of the problem. These are:

$$M_{ij} = \int_{\Omega} \psi_i \psi_j dx, \quad \text{for } i, j = 1, 2, \dots, N \quad (19)$$

$$A_{ij} = \int_{\Omega} \nabla \psi_i \cdot \nabla \psi_j dx, \quad \text{for } i, j = 1, 2, \dots, N \quad (20)$$

$$P_i(\phi(t)) = \int_{\partial\Omega} \psi_i (\nabla (\sum_{j=1}^N \phi_j(t) \cdot n) \cdot n) ds \quad (21)$$

$$\overline{W'}(\phi(t))_{ij} = \int_{\Omega} W'(\sum_{j=1}^N \phi_j(t) \psi_j) \psi_i, \quad \text{for } j = 1, 2, \dots, N \quad (22)$$

Spatial discretization in vector-matrix notation reads as follows:

Find  $\mu_j(t)$ ,  $\phi_j(t)$  for  $j = 1, 2, \dots, N$  such that:

$$M\vec{\mu}(t) + P_i(\vec{\phi}) - A\vec{\phi}(t) - \frac{1}{\epsilon^2} \overline{W'}(\vec{\phi}(t)) = 0 \quad (23)$$

$$M \frac{d\vec{\phi}(t)}{dt} - P_i(\vec{\mu}) + \gamma A\vec{\mu}(t) = 0 \quad (24)$$

where  $t \in (0, T]$ .

The presence of the term arising from the double well potential, as well as the boundary integral term account for the nonlinearity of the problem, if we choose a fully implicit time stepping scheme. Otherwise, one may choose to consider the two terms calculated at the "previous" time point, thus making the scheme explicit. The following chapter illustrates in a more detailed manner these concepts.

## 2 The temporal discretization

This chapter serves as a general outline of the available time schemes that can be applied to phase field models and presents some of the critical bounds concerning the characteristic parameters of the modelling. Here we follow [10]. In the consideration of time-discrete schemes, we are concerned with the following properties:

1. the order of accuracy of the scheme,
2. the stability of the algorithm,
3. the solvability of the time-discrete equations.

In the context of linear problems, stability is associated with the decay of the time-discrete solution with time, a feature also attained by the exact solution of stable linear problems. When the stability of the time discrete solution is achieved independently of the time-step  $dt = \tau$ , the time-integration scheme is said to be unconditionally stable. If stability holds under some constraint (e.g., on the time-step size), then the scheme is said to be conditionally stable. Explicit time integration algorithms are always conditionally stable, while implicit schemes might be unconditionally stable.

For nonlinear problems, the situation is more complicated than for linear equations due to the several notions of stability (Lyapunov, asymptotical, exponential) that may be defined for different problems and due to the fact that unconditionally stable schemes is not, as in the linear case, identical to making the algorithm implicit. Because of the energetic structure behind phase-field models, natural notions of stability are those related to free-energy dissipation. In particular, a numerical scheme is said to be unconditionally energy- (or gradient-, or nonlinearly) stable if:

$$E(\phi_{n+1}) - E(\phi_n) \leq 0 \quad \text{for all } n \geq 0. \quad (25)$$

In other words, the scheme preserves the energy-dissipative property of the underlying model, in the sense that it dissipates energy at each time step. Analogously to the linear case, if (25) holds under some constraint, then the scheme is said to be conditionally energetically stable.

In analyzing time-integration schemes for phase-field theories, one needs to be specific about the smoothness of the particular chosen double well function  $W(\phi)$ . Two common assumptions are:

- **(A1)**  $W \in C^0[a, b] \cap C^2(a, b)$  with  $-\infty \leq a < b \leq \infty$ , and  $W''$  is bounded below, i.e.,  $W$  is continuous on the bounded interval  $[a, b]$  and at least twice differentiable on the open interval  $(a, b)$ , and there is a constant  $\kappa_W > 0$  such that

$$W''(\phi) \geq -\kappa_W \quad \text{for all } \phi \in (a, b). \quad (26)$$

- **(A2)**  $W \in C^{2,1}(\mathbb{R})$ , i.e.,  $W''$  is globally Lipschitz continuous. This means that there is a constant  $L_W > 0$  such that

$$|W''(\phi)| \leq L_W \quad \text{for all } \phi \in \mathbb{R}. \quad (27)$$

Note that if  $W$  satisfies **(A2)**, then it also satisfies **(A1)** (with  $a = -\infty$ ,  $b = \infty$ , and  $\kappa_W = L_W$ ), but not vice versa. In particular, the classical quartic potential

$$W(\phi) = \frac{1}{4}(1 - \phi^2)^2 \quad (28)$$

satisfies **(A1)** with  $a = -\infty$  and  $b = \infty$ , but it does not satisfy **(A2)**. The logarithmic potential

$$W(\phi) = \frac{1}{2} \left( (1 + \phi) \log \left( 1 + \frac{\phi}{2} \right) + (1 - \phi) \log \left( 1 - \frac{\phi}{2} \right) + \theta(1 - \phi^2) \right) \quad (29)$$

satisfies **(A1)** with  $a = -1$  and  $b = 1$ , and it also does not satisfy **(A2)**. On the other hand, the truncated quartic potential

$$W(\phi) = \begin{cases} (\phi + 1)^2 & \text{if } \phi < -1 \\ \frac{1}{4}(1 - \phi^2)^2 & \text{if } \phi \in [-1, 1] \\ (\phi - 1)^2 & \text{if } \phi > 1 \end{cases} \quad (30)$$

satisfies **(A1)** (with  $a = -\infty$  and  $b = \infty$ ) and **(A2)**.

## 2.1 First-order accurate schemes

We now consider first-order schemes for the Cahn–Hilliard equation. All of the schemes are implicit in some sense, since explicit schemes for fourth-order parabolic problems are infeasible.

### 2.1.1 Backward Euler

The backward Euler method applied to the Cahn–Hilliard equation leads to the system:

$$\frac{\phi_{n+1} - \phi_n}{\tau} = \Delta \mu_{n+1} \quad (31)$$

$$\mu_{n+1} = W'(\phi_{n+1}) - \epsilon^2 \Delta \phi_{n+1} \quad (32)$$

This method is nonlinearly implicit because it requires the solution of a nonlinear system for the pair  $(\phi_{n+1}, \mu_{n+1})$ . Implicit schemes which are unconditionally linearly stable, such as the Backward Euler method, are generally conditionally stable for nonlinear problems. To see this, consider the energy difference:

$$E(\phi_{n+1}) - E(\phi_n) = \int_{\Omega} \left( W(\phi_{n+1}) - W(\phi_n) + \frac{1}{2} \epsilon^2 |\nabla \phi_{n+1}|^2 - \frac{1}{2} \epsilon^2 |\nabla \phi_n|^2 \right) dx \quad (33)$$

Given two real numbers  $u$  and  $v$  that enclose  $\xi$ , we can use a Taylor’s series expansion to show that:

$$W(u) - W(v) - W'(u)(u - v) = -\frac{1}{2} W''(\xi)(u - v)^2 \leq \kappa_W \frac{(u - v)^2}{2} \quad (34)$$

where the inequality holds due to assumption **(A1)**, which is valid for all the potentials  $W$  of interest. One then obtains:

$$E(\phi_{n+1}) - E(\phi_n) \leq \int_{\Omega} \left( W'(\phi_{n+1})(\phi_{n+1} - \phi_n) + \frac{\kappa_W}{2} (\phi_{n+1} - \phi_n)^2 + \frac{1}{2} \epsilon^2 |\nabla \phi_{n+1}|^2 - \frac{1}{2} \epsilon^2 |\nabla \phi_n|^2 \right) dx \quad (35)$$

$$= \int_{\Omega} \left( \mu_{n+1}(\phi_{n+1} - \phi_n) - \frac{\epsilon^2}{2} \nabla \phi_{n+1} \cdot \nabla (\phi_{n+1} - \phi_n) + \frac{\kappa_W}{2} (\phi_{n+1} - \phi_n)^2 \right) dx \quad (36)$$

$$+ \int_{\Omega} \left( \frac{1}{2} \epsilon^2 |\nabla \phi_{n+1}|^2 - \frac{1}{2} \epsilon^2 |\nabla \phi_n|^2 \right) dx \quad (37)$$

$$= -\tau \|\nabla \mu_{n+1}\|^2 + \frac{\kappa_W}{2} \|\phi_{n+1} - \phi_n\|^2 \quad (38)$$

$$- \frac{1}{2} \epsilon^2 \|\nabla(\phi_{n+1} - \phi_n)\|^2 \quad (39)$$

Next, we bound  $\|\phi_{n+1} - \phi_n\|_2^2$  using the equation for  $\phi_{n+1}$ :

$$\int_{\Omega} (\phi_{n+1} - \phi_n)^2 dx = -\tau \int_{\Omega} \nabla \mu_{n+1} \cdot \nabla (\phi_{n+1} - \phi_n) dx \quad (40)$$

$$\leq \tau \frac{1}{2\delta} \int_{\Omega} |\nabla \mu_{n+1}|^2 dx + \frac{\tau \delta}{2} \int_{\Omega} |\nabla(\phi_{n+1} - \phi_n)|^2 dx \quad (41)$$

where the last inequality holds for any  $\delta > 0$ . Finally, choosing  $\delta = \frac{2\epsilon^2}{\kappa_W \tau}$  gives:

$$E(\phi_{n+1}) - E(\phi_n) \leq -\tau \left( 1 - \frac{\kappa_W^2 \tau \epsilon^2}{8} \right) \int_{\Omega} |\nabla \mu_{n+1}|^2 dx \quad (42)$$

Therefore, if:

$$\tau < \frac{8\epsilon^2}{\kappa_W^2} \quad (43)$$

then (25) holds. In other words, the backward Euler scheme is conditionally energy stable. Furthermore, it can be shown that under the same time-step constraint, the nonlinear system (31)–(32) has a unique



solution for  $(\phi_{n+1}, \mu_{n+1})$  if condition (39) holds. The proof of this can be found in, for example, [8], and the underlying concept of the proof is applicable to other schemes.

To prove the existence of a solution, one demonstrates that the system represents the necessary condition (Euler-Lagrange equation) corresponding to a minimization problem for a convex functional. Subsequently, to prove the uniqueness of a solution, one follows similar steps to those used in establishing the energy stability mentioned earlier. It's worth noting that, since  $\epsilon$  is generally very small, condition (39) imposes a severe constraint on the allowed time-step size.

### 2.1.2 First-order semi-implicit method

A popular scheme (Provatas and Elder, 2010) is the following first-order semi-implicit (or implicit/explicit) method:

$$\frac{\phi_{n+1} - \phi_n}{\tau} = \Delta \mu_{n+1} \quad (44)$$

$$\mu_{n+1} = W'(\phi_n) - \epsilon^2 \Delta \phi_{n+1} \quad (45)$$

Because it treats  $W'$  explicitly, it is a linear (or linearly-implicit) method requiring the solution of a linear system at each time step. The system can be written abstractly as:

$$B \begin{bmatrix} \mu_{n+1} \\ \phi_{n+1} \end{bmatrix} = \begin{bmatrix} \phi_n \\ -W'(\phi_n) \end{bmatrix} \quad (46)$$

where  $B$  is the differential operator defined by:

$$B = \begin{bmatrix} -\tau \Delta & -I \\ -I & -\epsilon^2 \Delta \end{bmatrix} \quad (47)$$

Here,  $I$  denotes the identity operator. The linear system of differential equations (46) has a unique solution, independent of  $\tau$ . This follows from the coercivity estimate:

$$\int_{\Omega} \begin{bmatrix} \mu_{n+1} \\ \phi_{n+1} \end{bmatrix} \cdot B \begin{bmatrix} \mu_{n+1} \\ \phi_{n+1} \end{bmatrix} dx = \tau \|\nabla \mu_{n+1}\|^2 + \epsilon^2 \|\nabla \phi_{n+1}\|^2 \quad (48)$$

as well as mass conservation  $\int_{\Omega} (\phi_{n+1} - \phi_n) dx = 0$  and the condition  $\int_{\Omega} \mu_{n+1} dx = \int_{\Omega} W'(\phi_n) dx$ .

However, as may be expected, the method is only conditionally energy stable. In fact, we can only show conditional stability if  $W$  satisfies (A2). Let us assume that  $\xi$  is an undetermined point of the interval  $(0, 1)$ . Then,

$$E(\phi_{n+1}) - E(\phi_n) = -\tau \|\nabla \mu_{n+1}\|^2 + \frac{1}{2} \int_{\Omega} W''(\phi_{n+\xi}) (\phi_{n+1} - \phi_n)^2 dx - \frac{1}{2} \epsilon^2 \|\nabla(\phi_{n+1} - \phi_n)\|^2 \quad (49)$$

$$\leq -\tau \|\nabla \mu_{n+1}\|^2 + \frac{L_W}{2} \|\phi_{n+1} - \phi_n\|^2 - \frac{\epsilon^2}{2} \|\nabla(\phi_{n+1} - \phi_n)\|^2 \quad (50)$$

where  $\phi_{n+\xi} \approx \phi(\cdot, t_n + \xi\tau)$ . The inequality (50) is identical to (39) replacing  $\kappa_W$  with  $L_W$ . Therefore, following the same steps, leads to the similar constraint  $\tau < \frac{8\epsilon^2}{L^2 W}$  for energy stability.

### 2.1.3 Convex-Splitting Method

The stability issues for the backward Euler and semi-implicit methods originate from the nonconvexity of  $W(\phi)$ . A groundbreaking idea, which goes back to [11] and was popularized by [12], is to split  $W$  into a convex part and a concave part, i.e.,

$$W(\phi) = W_+(\phi) + W_-(\phi) \quad (51)$$

with  $W_+(\phi) \geq 0$  and  $W_-(\phi) \leq 0$ . Then, we treat  $W_+$  implicitly and  $W_-$  explicitly, as

$$\frac{\phi_{n+1} - \phi_n}{\tau} = \Delta\mu_{n+1} \quad (52)$$

$$\mu_{n+1} = W'_+(\phi_{n+1}) + W'_-(\phi_n) - \epsilon^2 \Delta\phi_{n+1} \quad (53)$$

Using Taylor's formulas, we have

$$W_+(\phi_{n+1}) = W_+(\phi_n) + W'_+(\phi_{n+1})(\phi_{n+1} - \phi_n) - \frac{1}{2}W''_+(\phi_{n+\xi})(\phi_{n+1} - \phi_n)^2 \quad (54)$$

$$W^-(\phi_{n+1}) = W^-(\phi_n) + W^-(\phi_n)(\phi_{n+1} - \phi_n) + \frac{1}{2}W''^-(\phi_n + \zeta)(\phi_{n+1} - \phi_n)^2 \quad (55)$$

where  $\xi, \zeta \in (0, 1)$ . The energy difference is now

$$E(\phi_{n+1}) - E(\phi_n) = -\tau \|\nabla\mu_{n+1}\|^2 - \frac{1}{2} \int_{\Omega} (W''_+(\phi_{n+\xi}) - W''_-(\phi_{n+\zeta})) (\phi_{n+1} - \phi_n)^2 dx - \frac{1}{2}\epsilon^2 \|\nabla(\phi_{n+1} - \phi_n)\|^2 \quad (56)$$

$$\leq -\tau |\nabla\mu_{n+1}|^2 - \frac{\epsilon^2}{2} |\nabla(\phi_{n+1} - \phi_n)|^2 \quad (57)$$

which shows the unconditional stability of the method. If  $W$  satisfies (A1), then the above convex splitting is non-unique, but it is always possible. For instance, defining

$$W^-(\phi) = -\kappa_W \frac{\phi^2}{2} \quad (58)$$

and subsequently setting  $W^+(\phi) = W(\phi) - W^-(\phi)$ . Unique solvability of the system follows by equivalence with a strictly-convex minimization problem. Hence, the convex-splitting scheme is both unconditionally stable and unconditionally solvable. If, in addition, (A2) applies, then a splitting is possible with  $W^+(\phi)$  being a quadratic polynomial, i.e., defining

$$W^+(\phi) = L \frac{W}{2} \phi^2 \quad (59)$$

and subsequently setting  $W^-(\phi) = W(\phi) - W^+(\phi)$ . In this case, the scheme becomes even linear.

## 2.2 Stability and Solvability Analysis for Second-order Schemes

### 2.2.1 Crank–Nicolson Method

The Crank–Nicolson method is defined as follows:

$$\frac{\phi_{n+1} - \phi_n}{\tau} = \Delta\mu_{n+\frac{1}{2}} \quad (60)$$

$$\mu_{n+\frac{1}{2}} = \frac{W'(\phi_{n+1}) + W'(\phi_n)}{2} - \epsilon^2 \Delta \frac{\phi_{n+1} + \phi_n}{2} \quad (61)$$

It requires the solution of a nonlinear system at each time step. Using the trapezoidal quadrature rule, we have

$$W(v) - W(u) = \int_u^v W'(s) ds = \frac{W'(u) + W'(v)}{2} (v - u) - \frac{1}{2} W'''(\xi) (v - u)^3 \quad (62)$$

where  $\xi$  is an unknown point that lies between  $u$  and  $v$ . Then, it can be shown that the energy difference is given by:

$$E(\phi_{n+1}) - E(\phi_n) = -\tau \|\nabla\mu_{n+1}\|^2 - \frac{1}{12} \int_{\Omega} W'''(\xi) (\phi_{n+1} - \phi_n)^3 dx \quad (63)$$

The sign of the last term in (63) cannot be controlled, making the method generally not unconditionally energy stable. Furthermore, the solvability of this method, corresponding to a nonconvex nonlinear system, also suffers from a time-step constraint,  $\tau \leq C\epsilon^2/\kappa_W^2$ , similar to the backward Euler scheme.

### 2.2.2 Second-order Semi-implicit Method

The second-order semi-implicit method is defined as:

$$\frac{\phi_{n+1} - \phi_n}{\tau} = \Delta\mu_{n+\frac{1}{2}} \quad (64)$$

$$\mu_{n+\frac{1}{2}} = W'(\phi_n) + \frac{1}{2}W''(\phi_n)(\phi_{n+1} - \phi_n) - \epsilon^2\Delta\frac{\phi_{n+1} + \phi_n}{2} \quad (65)$$

This method is linear and corresponds to the following system:

$$B \begin{bmatrix} \phi_{n+1} \\ \mu_{n+1} \end{bmatrix} = \begin{bmatrix} \phi_n - W'(\phi_n) + \frac{1}{2}W''(\phi_n)\phi_n - \frac{1}{2}\epsilon^2\Delta\phi_{n+1} \\ \phi_n \end{bmatrix} \quad (66)$$

where  $B_n$  is the differential operator defined by

$$B_n := \begin{bmatrix} -\tau\Delta & Id \\ -Id & \frac{1}{2}W''(\phi_n) - \frac{1}{2}\epsilon^2\Delta \end{bmatrix} \quad (67)$$

Because of the non-convexity of the potential,  $W''$  can have an arbitrary sign. Therefore, the method is conditionally uniquely solvable under a time-step constraint  $\tau < \frac{C\epsilon^2}{\kappa^2}W$ .

### 2.2.3 Secant Method

The secant method, designed to mimic the energy dissipation, is defined as:

$$\frac{\phi_{n+1} - \phi_n}{\tau} = \Delta\mu_{n+\frac{1}{2}} \quad (68)$$

$$\mu_{n+\frac{1}{2}} = DW(\phi_n, \phi_{n+1}) - \epsilon^2\Delta\frac{\phi_{n+1} + \phi_n}{2} \quad (69)$$

Here,  $DW(\phi, \psi)$  is the discrete variational derivative defined as:

$$DW(\phi, \psi) = \int_0^1 W'(\phi + s(\psi - \phi)) ds \quad (70)$$

Alternatively, the discrete variational derivative can be expressed as:

$$DW(\phi_n, \phi_{n+1}) = \begin{cases} \frac{W(\phi_{n+1}) - W(\phi_n)}{\phi_{n+1} - \phi_n} & \text{if } \phi_{n+1} \neq \phi_n \\ W'(\phi_n) & \text{if } \phi_{n+1} = \phi_n \end{cases} \quad (71)$$

This formulation explains the name of the method. By observing that

$$DW(\phi_n, \phi_{n+1})(\phi_{n+1} - \phi_n) = W(\phi_{n+1}) - W(\phi_n) \quad (72)$$

it can be deduced that the method is unconditionally energy stable, as indicated by the relation

$$E(\phi_{n+1}) - E(\phi_n) = -\tau\|\nabla\mu_{n+1}\|^2. \quad (73)$$

However, due to the non-convex nature of  $W$ , the nonlinear system (69)–(70) is only conditionally solvable (Elliott, 1989). The operator  $DW$  finds extensive use in the development of exact energy-preserving schemes. This method is unconditionally energy stable, but the solvability of the nonlinear system (68)–(69) is conditional. Several variants that avoid constructing the secant while maintaining stability are as follows:

1. Implicit Taylor Method:

$$DW(\phi_n, \phi_{n+1}) = W'(\phi_{n+1}) - \frac{1}{2}W''(\phi_{n+1})(\phi_{n+1} - \phi_n) + \frac{1}{3!}W'''(\phi_{n+1})(\phi_{n+1} - \phi_n)^2 \quad (75)$$

2. Method by Gomez and Hughes (2011):

$$DW(\phi_n, \phi_{n+1}) = \frac{1}{2} (W'(\phi_n) + W'(\phi_{n+1})) - \frac{1}{12} W'''(\phi_n)(\phi_{n+1} - \phi_n)^2 \quad (76)$$

These methods lead to the following energy change:

$$E(\phi_{n+1}) - E(\phi_n) = -\tau \|\nabla \mu_{n+1}\|^2 - \frac{1}{24} \int_{\Omega} W''''(\phi_{n+\xi})(\phi_{n+1} - \phi_n)^4 d\Omega, \quad \xi \in (0, 1) \quad (77)$$

The last term is negative or zero if  $W'''' \geq 0$ . This inequality holds for all potential functions. If the potential  $W$  does not satisfy the condition  $W'''' \geq 0$ , Gomez and Hughes (2011) [13] propose a splitting of  $W$  that achieves second-order accuracy and unconditional stability. Considering that the methods described in this section correspond to non-convex nonlinear systems, their solvability is conditional.

### 2.2.4 Second-order Convex Splitting

In an effort to achieve both unconditional stability and solvability, a second-order time-accurate convex-splitting scheme was proposed by Hu et al. (2009). The method is described by the following equations:

$$\frac{\phi_{n+1} - \phi_n}{\tau} = \Delta \mu_{n+\frac{1}{2}} \quad (74)$$

$$\mu_{n+\frac{1}{2}} = DW_+(\phi_{n+1}, \phi_n) + DW_-(\phi_n, \phi_{n-1}) - \frac{\varepsilon^2}{2} \Delta \frac{\phi_{n+1} + \phi_n}{2} \quad (78)$$

Where: -  $DW_+(\phi_{n+1}, \phi_n)$  is defined as:

$$DW_+(\phi_{n+1}, \phi_n) = \int_0^1 W'(\phi_n + s(\phi_{n+1} - \phi_n)) ds \quad (79)$$

-  $DW_-(\phi_n, \phi_{n-1})$  is defined as:

$$DW_-(\phi_n, \phi_{n-1}) = \frac{3}{2} W'_-(\phi_n) - \frac{1}{2} W'_-(\phi_{n-1}) \quad (80)$$

This method employs a secant treatment of the convex part and a two-step second-order backward difference treatment of the concave part. While this method is unconditionally solvable, it does not meet the criteria for unconditional stability. A less restrictive condition, referred to as weak energy stability (Hu et al., 2009), may be established if  $W_-$  is a quadratic polynomial, which holds for many potential functions. An alternative approach is the multistep scheme proposed in (Guillén-González and Tierra, 2013), which, however, is limited to quartic potentials. This alternative scheme is linear, unconditionally energy stable (with a modified energy statement), and unconditionally uniquely solvable. The above and the following references can be found in the main [10]

### 2.3 Stabilization

Most second-order linear schemes suffer from conditional stability and/or conditional solvability. As proposed by Wu et al. (2014), these issues can be stabilized if  $W$  satisfies (A2). For example, the stabilized semi-implicit scheme is given as follows:

$$\frac{\phi_{n+1} - \phi_n}{\tau} = \Delta \mu_{n+\frac{1}{2}} \quad (75)$$

$$\mu_{n+\frac{1}{2}} = W'(\phi_n) + \frac{1}{2} W''(\phi_n)(\phi_{n+1} - \phi_n) - \frac{\varepsilon^2}{2} \Delta \frac{\phi_{n+1} + \phi_n}{2} - \beta \tau \Delta(\phi_{n+1} - \phi_n) \quad (82)$$

Here,  $\beta$  is the stabilization parameter. Such terms are also referred to as artificial viscosity and are useful in many applications (see, e.g., Labovsky et al., 2009; Jansen et al., 2000). For a stabilization of the extended Crank–Nicolson method, refer to Gomez and Hughes (2011).

Using Taylor's formula, it can be shown that:

$$\begin{aligned}
E(\phi_{n+1}) - E(\phi_n) &= -\tau \|\nabla \mu_{n+1}\|^2 + \frac{1}{2} \int_{\Omega} (W''(\xi) - W''(\phi_n)) (\phi_{n+1} - \phi_n)^2 d\Omega \\
&\quad - \beta \tau \|\nabla(\phi_{n+1} - \phi_n)\|^2
\end{aligned} \tag{76}$$

Then, assuming that  $W$  satisfies (A2):

$$\begin{aligned}
E(\phi_{n+1}) - E(\phi_n) &\geq -\tau \|\nabla \mu_{n+1}\|^2 + L_W \|\phi_{n+1} - \phi_n\|^2 \\
&\quad - \beta \tau \|\nabla(\phi_{n+1} - \phi_n)\|^2 \\
&\geq -\tau \left(1 - \frac{L_W}{2\delta}\right) \|\nabla \mu\|^2 - \tau \left(\beta - \frac{L_W \delta}{2}\right) \|\nabla(\phi_{n+1} - \phi_n)\|^2 \text{ (by Young's inequality with } 0 < \delta < \frac{L_W}{2}\text{)}.
\end{aligned} \tag{77}$$

Therefore, for  $\beta > \frac{L_W^2}{4}$ , one has unconditional energy stability. It is worth noting that unconditional solvability follows by mimicking the proof for the Backward Euler method, as described in the work of Elliott [8].

### 3 The Newton-Raphson procedure

In this section, we briefly discuss the simplest multidimensional root finding method, the Newton-Raphson method. This method provides an efficient means of converging to a root when a sufficiently good initial data is given but, when this is not feasible it can fail to converge, indicating, though not proving, that a nearby root does not exist. For our implementation the initial guess has to be the combined solution of the previous time step, which for the most cases will work well. For the contained description we do not pose the following thoughts with a mathematical rigour but rather with the more intuitive approach.

We consider  $N$  functional relations that need to be set to zero and are represented as:

$$F_i(x_1, x_2, \dots, x_N) = 0, \quad i = 1, 2, \dots, N.$$

In the neighborhood of vector  $x$ , each function  $F_i$  can be expanded using a Taylor series:

$$F_i(x + \delta x) = F_i(x) + \sum_{j=1}^N \frac{\partial F_i}{\partial x_j} \delta x_j + O(\delta x^2).$$

The matrix  $J$  of partial derivatives appearing in the previous equation is the Jacobian matrix, with entries:

$$J_{ij} \equiv \frac{\partial F_i}{\partial x_j}.$$

In matrix notation we have:

$$\mathbf{F}(\mathbf{x} + \delta \mathbf{x}) = \mathbf{F}(\mathbf{x}) + J \delta \mathbf{x}.$$

By neglecting terms of order  $\delta x^2$  and setting  $\mathbf{F}(\mathbf{x} + \delta \mathbf{x}) = 0$ , we obtain a set of linear equations for the corrections  $\delta \mathbf{x}$  that simultaneously move each function closer to zero:

$$J \cdot \delta \mathbf{x} = -\mathbf{F}.$$

The matrix equation is then solved and the corrections are then added to the solution vector:

$$\mathbf{x}_{\text{new}} = \mathbf{x}_{\text{old}} + \delta \mathbf{x}.$$

The process is iterated until convergence is achieved. In general, it is advisable to check the degree to which both functions and variables have converged. Once either reaches machine accuracy, the other is unlikely to change. In our problem the presence of the double well potential accounts for the non-linearity of the Cahn-Hilliard model and of the arising discrete system of algebraic equations. Using a Taylor's expansion of the vector field of equations around the combined solution vector we achieve a linear approximation of the system. At each (fixed) time step  $t_n$ , we employ this iterative algorithm to solve it.

Let us consider that a standard backward Euler scheme is applied and let  $S_n = (\vec{\mu}_n, \vec{\phi}_n)$  denote the combined vector of unknowns. We state the relations (23),(24) as:

$$F_{vec}^n(S_n) = 0. \tag{78}$$

where the residual  $F_{vec}^n$  is defined by:

$$F_{vec}^n(S_n)_i = M\vec{\mu}(t) + P_i(\vec{\phi}) - A\vec{\phi}(t) - \frac{1}{\epsilon^2} \overline{W}'(\vec{\phi}(t)) \quad \text{for } i = 1, 2, \dots, N \tag{79}$$

$$F_{vec}^n(S_n)_i = M \frac{d\vec{\phi}(t)}{dt} - P_i(\vec{\mu}) + \gamma A \vec{\mu}(t) \quad \text{for } i = N + 1, \dots, 2N \tag{80}$$

Assuming a reasonable initial guess  $S_{n,0}$  of the solution  $S_n = (\vec{\mu}, n\vec{\phi}_n)$ , we iteratively solve the linearized equation and update the solution vector as follows:

$$J(S_{n;s}) \Delta S_{n;s} = -F_{vec}^n(S_{n;s}), \tag{81}$$

$$S_{n;s+1} = S_{n;s} + \Delta S_{n;s}, \quad s = 0, 1, \dots \tag{82}$$

where the entries of the Jacobian matrix  $J$  are  $J_{i,j}(S_n) = \frac{\partial F_{\text{res}}^n}{\partial S_n^j}$ ,  $i, j = 1, 2, \dots, 2N$ .

The iteration process is stopped below a certain tolerance (for instance,  $\|\Delta S_n\|_2 < \epsilon$ ).

For the calculation of the entries of the Jacobian matrix  $J$ , we differentiate the residual vector with respect to the nodal unknowns of the current timestep and we have:

$$\frac{\partial(M\vec{\mu}(t) + P_i(\vec{\phi}) - A\vec{\phi}(t) - \frac{1}{\epsilon^2}\overline{W}'(\vec{\phi}(t)))}{\partial\mu_j} = M_{ij}, \quad (83)$$

$$\frac{\partial(M\vec{\mu}(t) + P_i(\vec{\phi}) - A\vec{\phi}(t) - \frac{1}{\epsilon^2}\overline{W}'(\vec{\phi}(t)))}{\partial\phi_j} = \frac{\partial P_i}{\partial\phi_j} + A_{ij} - \frac{1}{\epsilon^2} \frac{\partial\overline{W}'(\vec{\phi})}{\partial\phi_j}, \quad (84)$$

$$\frac{\partial(M\frac{d\vec{\phi}(t)}{dt} - P_i(\vec{\mu}) + \gamma A\vec{\mu}(t))}{\partial\mu_j} = -\frac{\partial P_i}{\partial\mu_j} + \gamma A_{ij}, \quad (85)$$

$$\frac{\partial(M\frac{d\vec{\phi}(t)}{dt} - P_i(\vec{\mu}) + \gamma A\vec{\mu}(t))}{\partial\phi_j} = \frac{1}{dt} M_{ij} \quad (86)$$

where  $M_{ij}$ ,  $A_{ij}$ , represent the entries of the mass and stiffness matrices  $M$ ,  $A$ , respectively.

For the derivative of the non-linear term  $W'(\vec{\phi}_n)$ , the dependence on the solution forces us to employ the chain rule:

$$\frac{\partial\overline{W}'(\phi_n)_i}{\partial\phi_{nj}} = \frac{\partial\overline{W}'}{\partial\phi_n} \frac{\partial\phi_n}{\partial\phi_{nj}} = ((3(\sum_{l=1}^N \phi_l\psi_l)^2 - 1)\psi_i, \psi_j) \quad (87)$$

Note, that for the time being we omit the calculation of the derivative of the boundary flux integral term, as for the two cases of the boundary conditions that we will examine, the treatment has to be specific.

Provided that the Jacobian is invertible and  $S_n$  is sufficiently close to the exact solution  $S^*$ , the procedure usually converges rapidly, namely, it holds:

$$\|S_{n+1} - X^*\| \leq L\|S_n - S^*\|^2 \quad (88)$$

## 4 The periodic problem

When considering periodic conditions in the context of the Cahn-Hilliard equation, it typically refers to solving this equation in a domain with periodic boundaries. This means that the material or system under investigation is assumed to exhibit periodic patterns of phase separation. This typically refers to a phenomenon in materials science or physics where two or more phases or components of a material segregate or separate from each other in a regular, repeating pattern. This can occur in various contexts, such as in materials with a periodic structure, under specific temperature and pressure conditions, or in the presence of external forces.

### 4.1 Statement of the problem

For this chapter we will consider that the unit cell in  $\Omega = \mathbb{R}^2$  is the characteristic domain of periodicity for our solution. Following [8] we state the periodic problem for the Cahn-Hilliard equation as:

$$\frac{\partial \phi}{\partial t} = \gamma \nabla \cdot (\nabla (-\epsilon^2 \nabla^2 \phi + W'(\phi))) \text{ in } \Omega \times (0, T), \quad (89)$$

$$D^j \phi|_{x=0} = D^j \phi|_{x=1}, \quad \text{for } j = 0, \dots, 3 \quad \text{on } \overline{\Omega} \times (0, T), \quad (90)$$

$$D^j \phi|_{y=0} = D^j \phi|_{y=1}, \quad \text{for } j = 0, \dots, 3 \quad \text{on } \overline{\Omega} \times (0, T), \quad (91)$$

$$\phi|_{t=0} = \phi_0 \text{ in } \Omega \quad (92)$$

Considering the problem set on a rectangle (or a unit square) the periodicity condition (90)–(91) forces the solution to attain the same values on opposite sides of the boundary:

$$\phi(0, y, t) = \phi(1, y, t), \quad \forall y \in \overline{\Omega}_y \times (0, T] \quad (93)$$

$$\phi(x, 0, t) = \phi(x, 1, t), \quad \forall x \in \overline{\Omega}_x \times (0, T] \quad (94)$$

These two relations will be used on the fully discrete scheme to impose explicitly the boundary conditions and also to justify that for the finite dimensional approximation we technically use a subspace of periodic basis functions.

### 4.2 The finite dimensional projection of the solution

We recall the previous definition of the weak formulation of our problem:

Find  $(\psi, \eta)$  such that  $\psi \in L^\infty(0, T; H^1(\Omega))$ ,  $\phi_t \in L^2(0, T; (H^1(\Omega))')$ , and  $\eta \in L^2(0, T; H^1(\Omega))$  satisfying the following variational formulation:

$$\int_{\Omega} \mu \eta \, dx + \int_{\partial \Omega} \eta (\nabla \phi \cdot n) \, ds - \int_{\Omega} \nabla \phi \cdot \nabla \eta \, dx - \frac{1}{\epsilon^2} \int_{\Omega} W'(\phi) \eta = 0 \quad (95)$$

$$\int_{\Omega} \frac{\partial \phi}{\partial t} \psi \, dx - \int_{\partial \Omega} \psi (\nabla \mu \cdot n) \, ds + \gamma \int_{\Omega} \nabla \mu \cdot \nabla \psi \, dx = 0 \quad (96)$$



where  $n$  denotes the surface normal vector.

We consider  $\{\psi_i\}_{i=1}^N$ , the biquadratic Lagrange polynomial functions, or any other choice, for the approximation subspace. Seeking approximations for  $\mu$  and  $\phi$  so that they match at the nodal point with our functions, we would once more begin with the following representations:

$$\mu_h(t) = \sum_{j=1}^N \mu_j(t) \psi_j \quad (97)$$

$$\phi_h(t) = \sum_{j=1}^N \phi_j(t) \psi_j \quad (98)$$

with  $2N$  time-dependent unknowns  $\mu_j(t)$ ,  $\phi_j(t)$  for  $j = 1, 2, \dots, N$  to be found.

At this point, the periodic setting of the problem, forces the same nodal values on the nodes of the opposing boundary sides, as we have identified the length of each dimension with the period length in the horizontal and the vertical directions.

To define the local-global node connectivity list (i.e, how the local 1-9 reference numbering corresponds to the global domain numbering) we shall now opt for down to top and left to right scanning of the mesh, as illustrated in Figure7. Namely if we have  $N_y$  nodes on  $x = 0$ ,  $N_x$  nodes on  $y = 0$  the ascending order of the numbering is:

$$N_{ij} = (j - 1)N_y + i, \quad j = 1, \dots, N_y \quad i = 1, \dots, N_x \quad (99)$$

For the  $N_{max} = N = N_x N_y$  grid the periodic conditions mean:

$$\phi_i = \phi_{N - N_y + i}, \quad i = 1, \dots, N_y \quad (100)$$

$$\phi_{(j-1)N_y + 1} = \phi_{jN_y}, \quad j = 1, \dots, N_x \quad (101)$$

And the same relations hold for  $\mu$  as a consequence of (90)–(91).

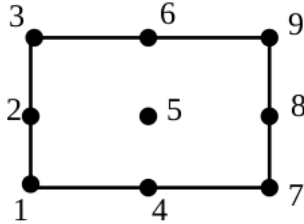


**Figure 4:** Down-top and Left-right numbering

The practical significance is that we now operate on a smaller number of unknowns, namely:  $N - N_x - N_y$ . The general representations shown above can now take a more specific form:

$$\bar{\mu}_h(t) = \sum_{j=1}^{N_y} \mu_j(\psi_j + \psi_{N-N_y+j}) + \sum_{i=2}^{N_x-1} \mu_{(i-1)N_y+1}(\psi_{(i-1)N_y+1} + \psi_{iN_y}) + \sum_{inner} \mu_j \psi_j \quad (102)$$

$$\bar{\phi}_h(t) = \sum_{j=1}^{N_y} \phi_j(\psi_j + \psi_{N-N_y+j}) + \sum_{i=2}^{N_x-1} \phi_{(i-1)N_y+1}(\psi_{(i-1)N_y+1} + \psi_{iN_y}) + \sum_{inner} \phi_j \psi_j \quad (103)$$

The representations (102),(103) actually state that a different set of basis functions (and hence test functions since we are on Galerkin methods territory) is best fit for the periodic setting.

We denote the new basis and test functions as:

$$\bar{\psi}_j = (\psi_j + \psi_{N-N_y+j}), \quad j = 1, \dots, N_y, \quad (104)$$

$$\bar{\psi}_{(i-1)N_y+1} = (\psi_{(i-1)N_y+1} + \psi_{iN_y}), \quad i = 2, \dots, N_x - 1 \quad (105)$$

$$\bar{\psi}_l = \psi_l, \quad l \text{ inner node} \quad (106)$$

### 4.3 The system's matrices

Based on the reduced (dimensionally) approximation of our functions and inserting relations (102)–(103) to the weak form of the problem, we calculate the necessary modifications of the matrices of the problem, to obtain the fully discrete scheme. To illustrate these modifications, the mass matrix now becomes:

For  $l$  inner node and  $j$  left side node we have:

$$\overline{M}_{lj} = \int_{\Omega} \overline{\psi}_l \overline{\psi}_j \, dx \quad (107)$$

$$= \int_{\Omega} \psi_l (\psi_j + \psi_{N-N_y+j}) \, dx \quad (108)$$

$$= \int_{\Omega} \psi_l \psi_j \, dx + \int_{\Omega} \psi_l \psi_{N-N_y+j} \, dx \quad (109)$$

$$= M_{lj} + M_{l;N-N_y+j} \quad (110)$$

For  $l$  inner node and  $m = (i-1)N_y + 1$  bottom side node we have:

$$\overline{M}_{lm} = \int_{\Omega} \overline{\psi}_l \overline{\psi}_{(i-1)N_y+1} \, dx \quad (111)$$

$$= \int_{\Omega} \psi_l (\psi_{(i-1)N_y+1} + \psi_{iN_y}) \, dx \quad (112)$$

$$= \int_{\Omega} \psi_l \psi_{(i-1)N_y+1} \, dx + \int_{\Omega} \psi_l \psi_{iN_y} \, dx \quad (113)$$

$$= M_{l(i-1)N_y+1} + M_{l;iN_y} \quad (114)$$

And the rest combinations follow in the same manner. These modifications apply also to the new stiffness matrix  $\overline{A}$ . Clearly the new matrices remain symmetric. The above modifications are inherited by the global system matrix presented in the previous chapter, as the mass, stiffness and the derivative matrix of the nonlinear term constitute the constructive blocks of the matrix.

#### 4.4 The nonlinear term

For the handling of the nonlinear term  $\overline{W'}(\overline{\phi}_h)$ , we notice that it equals to:

$$\int_{\Omega} \left( \sum_{j=1}^{N_y} \phi_j \overline{\psi}_j + \sum_{i=2}^{N_x-1} \phi_{(i-1)N_y+1} \overline{\psi}_{(i-1)N_y+1} + \sum_{inner} \phi_j \psi_j \right)^3 - \left( \sum_{j=1}^{N_y} \phi_j \overline{\psi}_j - \sum_{i=2}^{N_x-1} \phi_{(i-1)N_y+1} \overline{\psi}_{(i-1)N_y+1} \right) \overline{\psi}_i - \sum_{inner} \phi_j \psi_j \Big) \overline{\psi}_i \, da \quad (115)$$

The following remarks are critical to give us the correct representation of the non-linear term with the use of the modified basis:

1. The (real) inner product (integral) is linear in the second variable, so it can be split as a sum of integrals over the components of the new basis function  $\overline{\psi}_j$  (relations(104)–(105)). For instance we consider a function given by (104) and we have:

$$(W'(\overline{\phi}_h), \psi_j + \psi_{N-N_y+j}) = (W'(\overline{\phi}_h), \psi_j) + (W'(\overline{\phi}_h), \psi_{N-N_y+j}) \quad (116)$$

2. Each of these integrals can be rewritten as a sum of integrals over the composing elements of our domain.

$$\sum_e \int_{\Omega_e} W'(\overline{\phi}_h)(\psi_j + \psi_{N-N_y+j}) = \sum_e \int_{\Omega_e} W'(\overline{\phi}_h)(\psi_j) + \sum_e \int_{\Omega_e} W'(\overline{\phi}_h)(\psi_{N-N_y+j}) \quad (117)$$

3. On each element only the shape functions with support on the specific element remain nonzero in  $W'$ , resulting exactly in the form (per element) we had for the original shape functions  $\psi_j$ .

4. Finally the new component is the sum of the "periodically correspondent" components of the original base representation of the nonlinear term.

For instance, if we take  $i = 1, \dots, N_y$  (i.e, horizontal periodicity) we have:

$$\overline{W'}(\overline{\phi})_i = \overline{W'}(\phi)_i + \overline{W'}(\phi)_{N-N_y+i} \quad (118)$$

## 4.5 The boundary flux matrix

The last term we should carefully handle is the boundary integral term of the weak formulation. This affects the essential form of the weak formulation. We notice that for our simple rectangular domain we operate under a known orientation and with a known normal vector, on each side. Considering a counter-clockwise route of the boundary, we have:

$$\int_{\partial\Omega} \eta(\nabla\phi \cdot n) ds = \int_{\partial\Omega_B} \eta(\nabla\phi \cdot n) ds + \int_{\partial\Omega_R} \eta(\nabla\phi \cdot n) ds + \int_{\partial\Omega_T} \eta(\nabla\phi \cdot n) ds + \int_{\partial\Omega_L} \eta(\nabla\phi \cdot n) ds \quad (119)$$

$$= - \int_{\partial\Omega_B} \eta \frac{\partial\phi}{\partial y} ds + \int_{\partial\Omega_R} \eta \frac{\partial\phi}{\partial x} ds + \int_{\partial\Omega_T} \eta \frac{\partial\phi}{\partial y} ds - \int_{\partial\Omega_L} \eta \frac{\partial\phi}{\partial x} ds \quad (120)$$

The last relation is a consequence of the simple form of the normal vector on each side of the rectangle. For general domains more precise handling is needed. We would either opt for a polygonal approximation of the domain, or for a parametric representation of curved parts or surfaces of the boundary. For our problem we can insert in the last relation, the approximation of the solution along with the modified basis functions.

$$= - \int_{\partial\Omega_B} \bar{\psi}_i \sum_j \phi_j \frac{\partial\bar{\psi}_j}{\partial y} ds + \int_{\partial\Omega_R} \bar{\psi}_i \sum_j \phi_j \frac{\partial\bar{\psi}_j}{\partial x} ds + \int_{\partial\Omega_T} \bar{\psi}_i \sum_j \phi_j \frac{\partial\bar{\psi}_j}{\partial y} ds - \int_{\partial\Omega_L} \bar{\psi}_i \sum_j \phi_j \frac{\partial\bar{\psi}_j}{\partial x} ds \quad (121)$$

$$= \sum_j \phi_j \left( - \int_{\partial\Omega_B} \bar{\psi}_i \frac{\partial\bar{\psi}_j}{\partial y} ds + \int_{\partial\Omega_R} \bar{\psi}_i \frac{\partial\bar{\psi}_j}{\partial x} ds + \int_{\partial\Omega_T} \bar{\psi}_i \frac{\partial\bar{\psi}_j}{\partial y} ds - \int_{\partial\Omega_L} \bar{\psi}_i \frac{\partial\bar{\psi}_j}{\partial x} ds \right) \quad (122)$$

$$= \sum_j \phi_j \cdot Q_{ij} \quad (123)$$

with  $Q_{ij}$  denoting from now on the boundary flux matrix.

The essential remark is that the boundary flux matrix is zero in the periodic setting. Consider for instance a modified test function  $\bar{\psi}_i$  supported on the bottom and on the top due to periodicity. Then we have:

$$- \int_{\partial\Omega_B} \bar{\psi}_i \frac{\partial\bar{\psi}_j}{\partial y} ds + \int_{\partial\Omega_T} \bar{\psi}_i \frac{\partial\bar{\psi}_j}{\partial y} ds = - \int_0^1 (\bar{\psi}_i(s, 0) - \bar{\psi}_i(s, 1)) \frac{\partial\bar{\psi}_j}{\partial y} ds = 0 \quad (124)$$

## 4.6 The algorithm for the periodic problem

In this chapter we present the main steps of the approach, to provide a better understanding of the implementation aspects, that will be presented in a separate chapter. A contained description would constitute of the following steps:

1. Generate the domain discretization for the rectangle  $\Omega$  into 9-node elements, by choosing the desired element number per direction (x,y).

2. Determine the local-global node connectivity identification.

3. Create a time grid  $0 = t_0 < t_1 < t_2 < \dots < t_{n_{max}} = T$  on  $0 < t < T$  with time steps  $\Delta t_n = t_n - t_{n-1}$  for  $n = 1, 2, \dots, n_{max}$ . The time scheme is chosen to be a first order accurate, the Backward Euler or the Provatas-Elder scheme.

4. Choose the initial condition for the coupled variables  $\mu_0$  and  $\phi_0$ .

5. Start the time point loop. For  $t_n = 1, 2, \dots, n_{max}$  do:

6. Choose the starting guess  $S_{n,0} = (\mu_{n-1}, \phi_{n-1})$  and a desired tolerance value  $tol$  for the Newton-Raphson process.

8. Start the Newton iterative process. For  $iter = 1, 2, \dots, iter_{max}$  do:

9. Assemble the nonlinear term  $W'(\phi)$ , the  $N \times N$  Jacobian matrix  $J$  of the nonlinear term using now the original biquadratic basis functions  $\phi$ , with entries:

$$W'(\phi^{n,q})_i = \int_{\Omega} \left( \left( \sum_{l=1}^N \phi_l \psi_l \right)^3 - \sum_{l=1}^N \phi_l \psi_l \right) \psi_i dx, \quad l, i = 1, 2, \dots, N$$

$$J_{ij}^{n,q} = \int_{\Omega} \left( 3 \left( \sum_{l=1}^N \phi_l \psi_l \right)^2 - 1 \right) \psi_i \psi_j dx, \quad l = 1, 2, \dots, N$$

and the right handside vector  $F_{vec}^n$  as defined by (79)–(80).

10. Assemble the global stiffness matrix with the inherited modifications shown in (107)–(124) for the stationary system of each Newton cycle:

$$F_{jac} = \begin{bmatrix} \overline{M} & -J - \varepsilon^2 \overline{A} \\ \Delta t \overline{A} & \overline{M} \end{bmatrix} \quad (125)$$

11. Solve with the biconjugate gradient method (BiCGStab) the system:

$$F_{jac} \cdot \Delta S_{n,iter} = -F_{vec} \quad (126)$$

12. Update the solution guess and recover the boundary values of the solution on the right and top side (given that we have retained the left and bottom as main), as shown in relations (100)–(101):

$$S_{n,iter+1} = S_{n,iter} + \Delta S_{n,iter} \quad (127)$$

13. If the norm is below the tolerance value stop.

$$\|\Delta S_{n,iter}\|_2 < tol \quad (128)$$

14. End the Newton iteration loop.

15. Set the solution vectors of the reduced dimension  $\vec{\mu}_n$  and  $\vec{\phi}_n$ , with entries  $\mu_{n_i} = S_{n,iter_{i=1}^N}$  and  $\phi_{n_i} = S_{n,iter_{N+1}^{2N}}$  and extend back to the full dimension periodically.

16. End the time step loop in  $n$ .

17. Write the results.

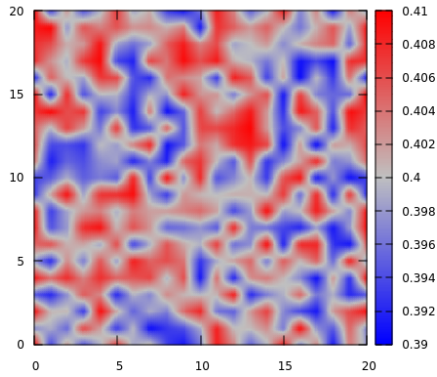
#### 4.6.1 Experiments-Results

Spinodal decomposition is the separation of a mixture of two or more components to the bulk regions of both. Bulk regions are defined as the regions purely occupied by one of the components. This decomposition phenomena occurs when a high temperature mixture of two or more alloys is cooled rapidly(quenching). For this experiment an initial condition with mean 0.4 was chosen which is perturbed under

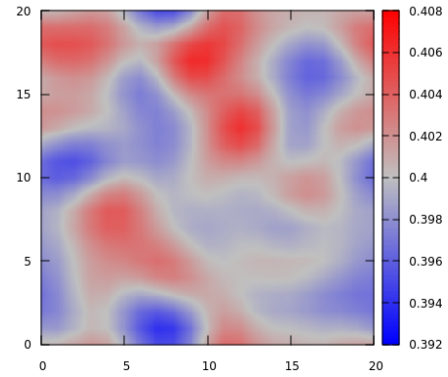
$$\phi_0 = 0.4 + 0.02(0.5 - r) \tag{129}$$

with  $r$  being a random number in  $[0, 1]$ . Here  $dt = 5 \times 10^{-9}$  constant throughout the simulation and  $\epsilon = 5 \times 10^{-2}$ . The phase portraits of Figure 5, depict the evolution of the initial state up to the latter stages of the coarsening and the separation of the two phases. Bulk regions are gradually formed until they reach a constant curvature profile.

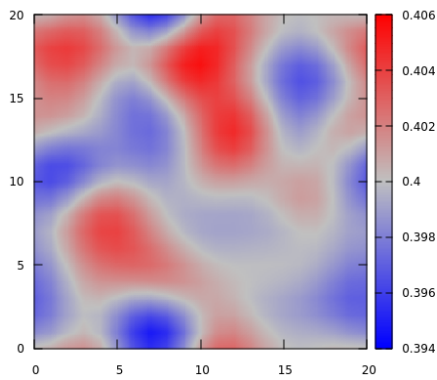




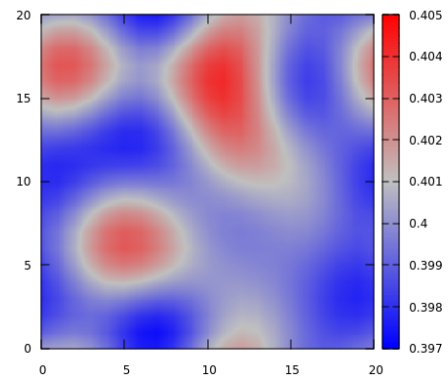
(a)  $t=0$



(b)  $t=500dt$



(c)  $t=1000dt$



(d)  $t=5000dt$

**Figure 5:** Evolution of the phase field on a 441-node domain. The phase portraits (a)–(e) illustrate the formation of the bulk regions from an initial mixture, along 3 time scales. Periodic conditions on both spatial directions have been assumed.

## 5 Phase-field model for wetting phenomena

### 5.1 Statement of the problem

Wetting phenomena typically involve a fluid–fluid interface advancing or receding on a solid substrate and a contact line formed at the intersection between the interface and the substrate. The wetting properties of the substrate determine to a large extent the behaviour of the fluids in the contact-line region. To account for wetting phenomena and contact lines on solid boundaries, the CH equation can be coupled to a wall boundary condition. Such models find applications in various situations, including microfluidic devices flow in porous media, rheological systems, and patterning of thin polymer films and others. Many of these applications are characterised by the presence of chemically heterogeneous substrates and complex geometries, which make their numerical simulation challenging. Throughout this chapter,  $\Omega \subset \mathbb{R}^2$  corresponds to a 2-dimensional rectangular domain,  $\partial\Omega$  denotes its boundary with outward unit normal vector  $\mathbf{n}$ ,  $\mathcal{S}$  is the solid substrate, and  $\mathcal{G} = \partial\Omega \setminus \mathcal{S}$ . The CH system we use to describe the dynamics of two immiscible fluids in contact with a solid substrate is a free-energy-based model. We consider systems with a free energy given by

$$E(\phi) := E_m(\phi) + E_w(\phi) \quad (130)$$

where the two terms,  $E_m$  and  $E_w$ , represent the mixing and wall components of the free energy, respectively. Here  $F_m(\phi) = \frac{1}{4}(\phi^2 - 1)^2$ , and  $F_w$  represents the energy cost or energy gain associated with the presence of a solid wall or substrate in contact with a liquid phase. This energy term accounts for the interactions between the fluid and the solid surface.

The specific wall free energy is a material property and depends on the nature of the solid-liquid interface. It is typically expressed in terms of surface tension or interfacial energy. It plays a crucial role in determining the wetting behavior of the liquid on the solid surface. When the specific wall free energy is lower than the bulk free energy of the system, the liquid tends to wet or spread on the surface. In contrast, when the specific wall free energy is higher than the bulk free energy, the liquid may not wet the surface, resulting in non-wetting behavior. It is taken to be a cubic polynomial:

$$F_w(\phi) = \frac{\sqrt{2}}{2} \cos \theta(x) \left( \frac{\phi^3}{3} - \phi \right) \quad (131)$$

where  $\theta = \theta(x)$  is the equilibrium contact angle, which can depend on the spatial position  $x$ . From the expression of the free energy, we calculate that, for a sufficiently smooth function  $\psi : \Omega \rightarrow \mathbb{R}$ :

$$\frac{d}{d\alpha} E(\phi + \alpha\psi) \Big|_{\alpha=0} = \int_{\Omega} \left( \frac{1}{\varepsilon} f_m(\phi) - \varepsilon\phi \right) \psi d\Omega + \int_{\partial\Omega} (f_w(\phi) + \varepsilon\nabla\phi \cdot \mathbf{n}) \psi d\sigma \quad (132)$$

with  $f_m = F'_m$  and  $f_w = F'_w$ , so the chemical potential is equal to

$$\mu := \frac{\delta E}{\delta\phi} = \frac{1}{\varepsilon} f_m(\phi) - \varepsilon\phi \quad (133)$$

and the natural boundary condition associated with the surface energy is

$$\varepsilon\nabla\phi \cdot \mathbf{n} = -f_w(\phi) = \frac{\sqrt{2}}{2} \cos \theta(x) (1 - \phi^2) \quad (134)$$

We assume that the dynamics of the system is governed by the CH equation,

$$\frac{\partial\phi}{\partial t} = \nabla \cdot (b(x)\nabla\mu) \quad (135)$$

where  $b(x)$  is a mobility parameter, assumed to be equal to one. The mass-conservation property holds:

$$\frac{d}{dt} M(\phi) := \frac{d}{dt} \int_{\Omega} \phi d\Omega = \int_{\partial\Omega} \nabla\mu \cdot \mathbf{n} d\sigma \quad (136)$$

The mass flux at the boundary can be specified enforcing certain condition on  $\nabla\mu \cdot \mathbf{n}$ . In particular, we will set  $\nabla\mu = 0$  at the solid boundary,  $\mathcal{S}$ . The system becomes:

$$\frac{\partial\phi}{\partial t} = \nabla \cdot (\nabla\mu) \quad (137)$$

$$\mu = \frac{1}{\varepsilon} f_m(\phi) - \varepsilon\Delta\phi, \quad x \in \Omega, t \in (0, T] \quad (138)$$

$$\varepsilon\nabla\phi \cdot \mathbf{n} = -f_w(\phi) \quad (139)$$

$$\nabla\mu \cdot \mathbf{n} = 0, \quad x \in \partial\Omega, t \in (0, T] \quad (140)$$

## 5.2 The weak formulation

The weak formulation of equations (141) to (145) is as follows: find  $(\phi, \mu)$  such that

$$\begin{aligned} \phi &\in L^\infty(0, T; H^1(\Omega)), \\ \frac{\partial\phi}{\partial t} &\in L^2(0, T; (H^1(\Omega))'), \\ \mu &\in L^2(0, T; H^1(\Omega)), \end{aligned} \quad (141)$$

and the following variational formulation is satisfied:

$$\left\langle \frac{\partial\phi}{\partial t}, \psi \right\rangle + (\nabla\mu, \nabla\psi) = 0, \quad \forall \psi \in H^1(\Omega) \text{ and almost everywhere for } t \text{ in } (0, T], \quad (142)$$

$$(\mu, \eta) = \varepsilon(\nabla\phi, \nabla\eta) + \frac{1}{\varepsilon}(f_m(\phi), \eta) + (f_w(\phi), \eta)_{\partial\Omega}, \quad \forall \eta \in H^1(\Omega) \text{ and almost everywhere for } t \text{ in } (0, T] \quad (143)$$

## 5.3 The temporal discretization and the algorithm

For the problem of this chapter we opt again for a standard backward Euler scheme that can be combined with some convex splitting scheme for the potential term to ensure unconditional stability and convergence as shown in the first chapter. For a more recent review of new numerical schemes proposed for the wetting phenomena that arise in the context of the Cahn Hilliard equation we refer to [14]. As shown in the previous chapter we have to handle a nonlinear system of equations on each timepoint using the Newton-Raphson method. One difference of the implementation aspect of the problem has to do with the boundary integral term:

$$\int_{\partial\Omega} \eta(1 - \phi^2) ds \quad (144)$$

arising from the wall energy. For the cases we examine we have a simple form for this term as our domain is a rectangle and we know explicitly the normal vector on each side. This new term has to be added to the residual vector and is calculated as a sum of contributions of four integral terms each one representing the integration on the corresponding boundary line (bottom, right, top, left):

$$\int_{\partial\Omega} \eta(1 - \phi^2) ds = \int_{\partial\Omega_b} \eta(1 - \phi^2) ds + \int_{\partial\Omega_r} \eta(1 - \phi^2) ds + \int_{\partial\Omega_t} \eta(1 - \phi^2) ds + \int_{\partial\Omega_l} \eta(1 - \phi^2) ds \quad (145)$$

Each of these four integrals is calculated as a sum over the elements whose one side intersects the corresponding boundary line:

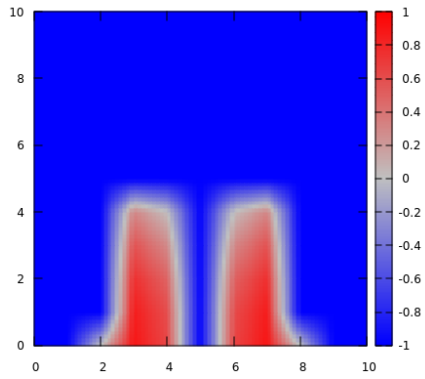
$$\int_{\partial\Omega_l} \eta(1 - \phi^2) ds = \sum_e \int_{\partial\Omega_e} \eta(1 - \phi^2) ds, \quad \text{where } \partial\Omega_e \cap l \neq \emptyset \quad (146)$$

### 5.3.1 Experiments-Results

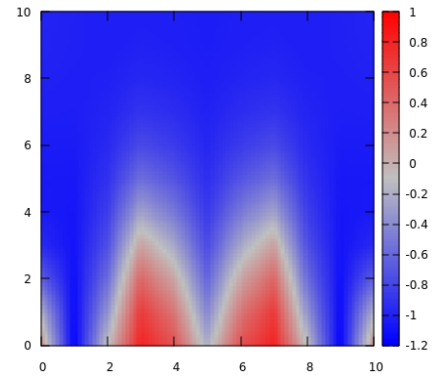
Here, we study the coalescence of two adjacent sessile droplets as they spread on a flat substrate. For the simulation, we used the initial condition:

$$\phi(x, y, 0) = 1 - \tanh\left(\frac{\sqrt{(x - x_1)^2 + y^2} - r^2}{\sqrt{2\varepsilon}}\right) - \tanh\left(\frac{\sqrt{(x - x_2)^2 + y^2} - r^2}{\sqrt{2\varepsilon}}\right)$$

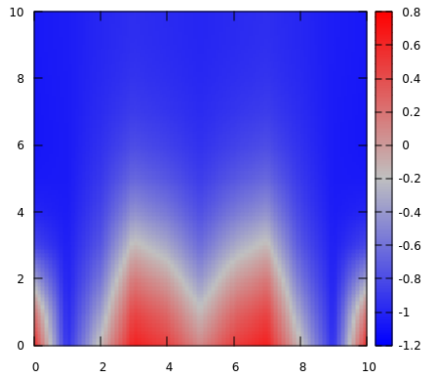
in the domain  $[0, 2] \times [0, 0.5]$ , with  $x_1 = 0.65$ ,  $x_2 = 1.35$ ,  $r = 0.25$ , and at the boundary, we imposed a uniform contact angle,  $\theta = \pi/4$  and  $\theta = 3\pi/4$  respectively, using the wall energy. Figures 10 and 11 depict the evolution of the phase field during the simulation for the two cases. Here  $e = 10^{-1}$  and the timestep was considered fixed  $dt = 5 \times 10^{-7}$  and  $10^4$  steps where applied.



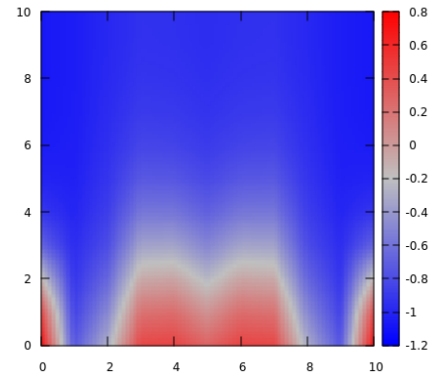
(a)  $t=0$



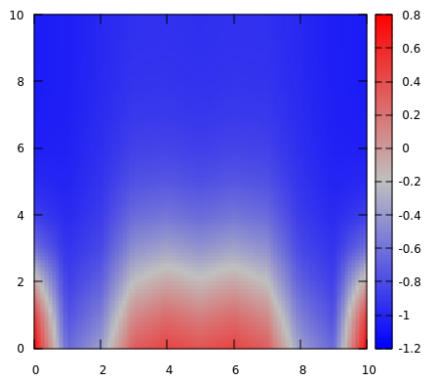
(b)  $t=1000dt$



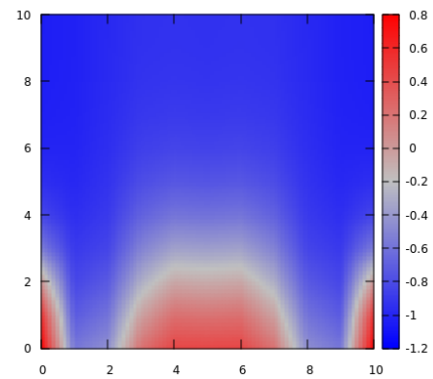
(c)  $t=3000dt$



(d)  $t=6000dt$

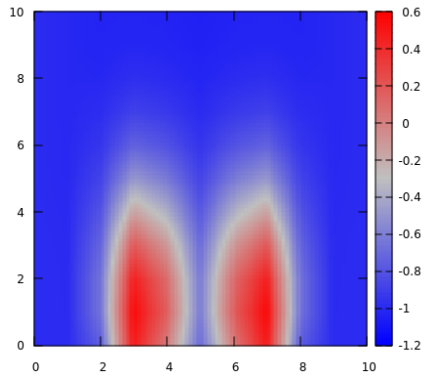


(e)  $t=8000dt$

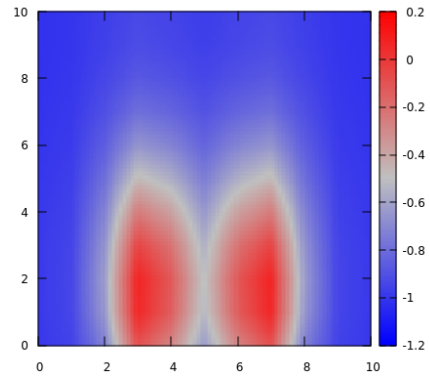


(f)  $t=10000dt$

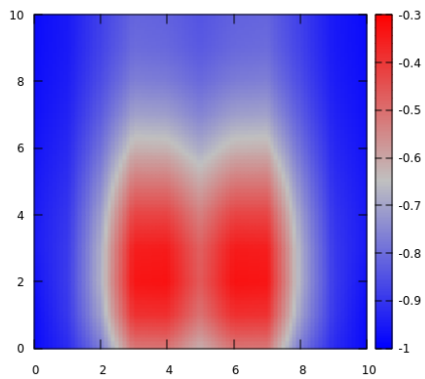
**Figure 6:** Evolution of phase field for  $\theta = \pi/4$ . The red region represents the region where the phase variable is equal to 1 and the blue the region where it equals  $-1$ . The hydrophilic setting illustrates the gradual merging of the two droplets as a result of surface tension.



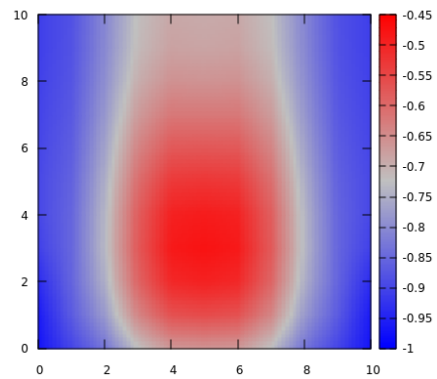
(a)  $t=1000dt$



(b)  $t=000dt$



(c)  $t=6000dt$



(d)  $t=10000dt$

**Figure 7:** Evolution of phase field for  $\theta = 3\pi/4$

## 6 Conclusions and future directions for the development of the code

The numerical methods for phase transition problems is a rich subject whose perspectives can be reflected on the future development directions of the current implementation. Contemporary methods besides the use of the standard finite element methods, as well as error analysis and convergence estimates can be found in the articles presented in references [15], [16], [17], [18], [19], [20], [21], [22], [23], [24], [25], [26]. In this work we used a standard backward Euler scheme along with the mixed finite element formulation of the Cahn-Hilliard equation, with periodic conditions. We also employ the same standard approach in the effort to capture the dynamics of the wetting phenomena that are described on the relevant chapter. The basic implementation that is presented in the appendix, is not optimized by any means and it only serves as a general solving tool that can easily be adapted to facilitate the higher accuracy, and better overall second order schemes that we briefly reviewed. The results that are depicted on the corresponding chapters aim to justify only that the certain implementation can produce valid results on small meshes(i.e with few nodes), that capture the essential stages of phase separation, and the rate of the energy decay etc. We stress that this implementation is not meanted to be used for serious applications, where a more optimized design would be mandatory. However we can outline the main directions, over which a future development-research effort should focus.

The main effort should focus on exploitting the second order schemes for the higher accuracy and for the better stability and solvability properties they present. Secondly one has to take into account that the different stages of the morphological evolution of the phase field occur at different time scales, indicating the need of an adaptive time step approach. For example, in the spinodal decomposition simulation, an initial random perturbation evolves on a fast time scale and later coarsening evolves on a very slow time scale. Therefore, if a uniform small time step is used to capture the fast dynamics, the computation is very costly. On the other hand, if a uniform large time step is used, fast time evolutions may be overlooked. Hence, it is essential to use an adaptive time step method to simulate phenomena with multiple time scales. Thirdly one has to take into account that "stiff" systems may occur and for these cases a wide range of preconditioning strategies can be employed to reduce the condition number of the system that has to be solved on each Newton cycle. For these strategies we refer to [27] Along with these aspects, crucial would be the modification of the classical Newton-Raphson procedure, to an inexact iterative scheme or to a globally convergent process like the line search or the multidimensional secant method (Broyden's Method, etc). To improve the performance it would be mandatory to exploit techniques of the sparse matrix formulations replacing costly computations with more efficient matrix to vector action when needed. For instance, one can exploit the computational gains that the Compressed Row Storage (CRS) format of the global stiffness matrix would provide. Paired with these should be the appropriate modifications of the Linear System Solvers that one can use. The easiest effort would be to modify an incomplete LU factorization process and solver, to factorize and solve (CRS) systems. This direct-solver approach can become efficient when handling "small" systems, but for serious applications a suitable modification of a more advanced iterative solver like GMRES would be obligatory. A very useful library written in FORTRAN for ideas like the above can be found in Y.Saad's work, the open SPARSKIT library. Finally of a more contemporary significance would be the effort to couple these modifications with the flow equations, to develop a tool for the Cahn-Hilliard-Navier-Stokes problem. We illustrate briefly some notes for these directions.

### 6.0.1 Adaptive time stepping

For the general outline of the techniques presented in this chapter we follow [28] and the references therein. A proposed adaptive time-stepping method using a criterion related to a residual of the discrete energy law

$$\frac{dE(\varphi)}{dt} = - \int_{\Omega} |\nabla\mu(x,t)|^2 dx. \quad (147)$$

is the following:

Given  $\varphi_n, \varphi_{n-1}, 1/t_n, 1/t_{n-1}$ , and a parameter  $\theta > 1$ , chosen to be  $\theta = 1.1$ , the method is as follows:

**Step 1.** Compute  $\varphi_{n+1}$  and obtain

$$R_{n+1} := E(\varphi_{n+1}) - E(\varphi_n) \frac{1}{t_n} + \int_{\Omega} |\nabla \mu_{n+1}|^2 dx. \quad (148)$$

**Step 2.** If  $|R_{n+1}| > \text{resmax}$ , take  $1/t_n = 1/t_n/\theta$  and go to Step 1.

**Step 3.** If  $|R_{n+1}| < \text{resmin}$ , take  $1/t_{n+1} = \theta \cdot 1/t_n$ .

Here, a trial and error choice of  $\text{resmax}$  and  $\text{resmin}$  was used.

An adaptive time-stepping method using the time derivative of the total energy was considered in [?]; that is,

$$\Delta t = \max(\Delta t_{min}, \frac{\Delta t_{max}}{\sqrt{(1 + \alpha |E'(t)|^2)}}), \quad (8)$$

where the constant  $\alpha$  is chosen to regulate the adaptivity. A large value of  $|E'(t)|$  leads to a small time step, whereas a small  $|E'(t)|$  value yields a large time step.

The following adaptive time-stepping technique was developed in [?]:

**Step 1.** Calculate  $e = \frac{\|\varphi_{n+1}^{\text{BE}} - \varphi_{n+1}^{\alpha}\|_{\alpha}}{\|\varphi_{n+1}^{\alpha}\|_{\alpha}}$ , where  $\varphi_{n+1}^{\text{BE}}$  and  $\varphi_{n+1}^{\alpha}$  are the numerical solutions using the backward Euler method and a second-order generalized- $\alpha$  method with  $\Delta t^n$ , respectively.

**Step 2.** If  $e > \text{tol}$ , then reset the time step size  $\Delta t^n = \rho \sqrt{\frac{\text{tol}}{e}} \cdot \Delta t^n$  and return to Step 1, where  $\rho = 0.9$  and  $\text{tol} = 10^{-3}$  are used. Otherwise, set  $\Delta t^{n+1} = \rho \sqrt{\frac{\text{tol}}{e}} \cdot \Delta t^n$ .

To equally distribute the locally computable discretization error, the authors in [?] proposed the following algorithm:

**Step 1.** The global relative time discretization error estimate is defined by

$$e = \frac{\|\varphi_{n+1} - \hat{\varphi}_{n+1}\|_{\Delta t^n}}{\max(\|\varphi_{n+1}\|, \|\hat{\varphi}_{n+1}\|)}, \quad (150)$$

where  $\varphi_{n+1}$  and  $\hat{\varphi}_{n+1}$  are the numerical solutions obtained by taking two time steps of size  $\Delta t^n/2$  and a single time step of size  $\Delta t^n$  from  $\varphi_n$ , respectively.

**Step 2.** If  $e < e_{\text{MAX}}$ , then set

$$\Delta t^{n+1} = \Delta t^n \left( \frac{e_{\text{tol}}}{e} \right)^{1/p}, \quad (151)$$

where  $e_{\text{MAX}}$  is a target error tolerance and  $p$  is the global convergence rate of the time-stepping algorithm being used. If  $e \geq e_{\text{MAX}}$ , then that time step is rejected and go to Step 1, and recalculated with halving, i.e.,  $\Delta t^n = \Delta t^n/2$ .

Also the authors in [?] suggest an adaptive time-stepping scheme based on the convergence behavior of Newton-Raphson iterations.

## 6.0.2 Broyden's Method

One drawback of the classical Newton's method is that the Jacobian matrix calculations in many problems is expensive, or even not feasible. For this reason a series of methods under the general name of secant methods provide cheap approximations to the Jacobian. The most popular of these methods is Broyden's method.

Let us denote the approximate Jacobian by  $B$ . Then the  $i$ th quasi-Newton step  $\delta x_i$  is the solution of:

$$B_i \cdot \delta x_i = -F_i$$

where  $\delta x_i = x_{i+1} - x_i$  (cf. equation 9.7.3). The quasi-Newton or secant condition is that  $B_{i+1}$  satisfies:

$$B_{i+1} \cdot \delta x_i = \delta F_i$$



where  $\delta F_i = F_{i+1} - F_i$ . This is a generalization of the one-dimensional secant approximation to the derivative,  $\delta F/\delta x$ . However, the previous equation does not determine  $B_{i+1}$  uniquely in more than one dimension.

Many different auxiliary conditions to pin down  $B_{i+1}$  have been explored, but the best-performing algorithm in practice results from Broyden's formula. This formula is based on the idea of getting  $B_{i+1}$  by making the least change to  $B_i$  consistent with the secant equation. Broyden showed that the resulting formula is:

$$B_{i+1} = B_i + \frac{\delta F_i - B_i \cdot \delta x_i}{\delta x_i \cdot \delta x_i} \delta x_i \otimes \delta x_i \cdot \delta x_i$$

Early implementations of Broyden's method used the Sherman-Morrison formula, to invert the last equation analytically:

$$B_{i+1}^{-1} = B_i^{-1} + \frac{(\delta x_i - B_i^{-1} \cdot \delta F_i) \otimes \delta x_i \cdot B_i^{-1}}{\delta x_i \cdot B_i^{-1} \cdot \delta F_i}$$

Then instead of solving exactly, for example, LU decomposition may be employed, to determine  $\delta x_i = -B_i^{-1} \cdot F_i$  by matrix multiplication in  $O(N^2)$  operations.

Since  $B$  is not the exact Jacobian, we are not guaranteed that  $\delta x$  is a descent search direction. Thus, the line search algorithm can fail to return a suitable step if  $B$  wanders far from the true Jacobian. In this case, we reinitialize  $B$ . Like the secant method in one dimension, Broyden's method converges superlinearly once you get close enough to the root. Embedded in a global strategy, it is almost as robust as Newton's method and often needs far fewer function evaluations to determine a zero. Note that the final value of  $B$  is not always close to the true Jacobian at the root, even when the method converges.

## References

- [1] J. W. Cahn and J. E. Hilliard, “Free energy of a nonuniform system. i. interfacial free energy,” *Journal of Chemical Physics*, vol. 28, pp. 258–267, 1958.
- [2] J. W. Cahn, “On spinodal decomposition,” *Acta Metallurgica*, vol. 9, no. 9, pp. 795–801, 1961.
- [3] V. Badalassi, H. Ceniceros, and S. Banerjee, “Computation of multiphase systems with phase field models,” *Journal of Computational Physics*, vol. 190, no. 2, pp. 371–397, 2003.
- [4] J. Zhu, L. Chen, and J. Shen, “Morphological evolution during phase separation and coarsening with strong inhomogeneous elasticity,” *Modelling and Simulation in Materials Science and Engineering*, vol. 9, pp. 499–511, Nov. 2001.
- [5] V. Mohammadi and M. Dehghan, “Simulation of the phase field cahn–hilliard and tumor growth models via a numerical scheme: Element-free galerkin method,” *Computer Methods in Applied Mechanics and Engineering*, vol. 345, pp. 919–950, 2019.
- [6] S. Zhou and M. Wang, “Multimaterial structural topology optimization with a generalized cahn–hilliard model of multiphase transition,” *Structural and Multidisciplinary Optimization*, vol. 33, pp. 89–111, 02 2007.
- [7] S. Tremaine, “On the origin of irregular structure in saturn’s rings,” *The Astronomical Journal*, vol. 125, pp. 894 – 901, 2002.
- [8] C. M. Elliott, *The Cahn-Hilliard Model for the Kinetics of Phase Separation*, pp. 35–73. Basel: Birkhäuser Basel, 1989.
- [9] D. Lee, J. Y. Huh, D. Jeong, J. Shin, A. Yun, and J. Kim, “Physical, mathematical, and numerical derivations of the cahn–hilliard equation,” *Computational Materials Science*, vol. 81, pp. 216–225, 2014.
- [10] H. Gomez and K. van der Zee, *Computational Phase-Field Modeling*. 11 2015.
- [11] C. M. Elliott and A. M. Stuart, “The global dynamics of discrete semilinear parabolic equations,” *SIAM Journal on Numerical Analysis*, vol. 30, pp. 1622–1663, 1993.
- [12] D. J. Eyre, “Unconditionally gradient stable time marching the cahn-hilliard equation,” *MRS Proceedings*, vol. 529, p. 39, 1998.
- [13] H. Gomez and T. J. Hughes, “Provably unconditionally stable, second-order time-accurate, mixed variational methods for phase-field models,” *Journal of Computational Physics*, vol. 230, no. 13, pp. 5310–5327, 2011.
- [14] B. Aymard, U. Vaes, M. Pradas, and S. Kalliadasis, “A linear, second-order, energy stable, fully adaptive finite element method for phase-field modelling of wetting phenomena,” *Journal of Computational Physics: X*, vol. 2, p. 100010, 2019.
- [15] P. K. Chan and A. D. Rey, “A numerical method for the nonlinear cahn-hilliard equation with nonperiodic boundary conditions,” *Computational Materials Science*, vol. 3, no. 3, pp. 377–392, 1995.
- [16] M. Fernandino and C. Dorao, “The least squares spectral element method for the cahn–hilliard equation,” *Applied Mathematical Modelling*, vol. 35, no. 2, pp. 797–806, 2011.
- [17] W. Wang, Z. Wang, and Z. li, “Long time h a s stability of a classical scheme for cahn-hilliard equation with polynomial nonlinearity,” *Applied Numerical Mathematics*, vol. 165, 02 2021.
- [18] G. Vandin, D. Marenduzzo, A. Goryachev, and E. Orlandini, “Curvature-driven positioning of turing patterns in phase-separating curved membranes,” *Soft Matter*, vol. 12, 03 2016.
- [19] H. Garcke and P. Knopf, “Weak solutions of the cahn-hilliard system with dynamic boundary conditions: A gradient flow approach,” 10 2018.

- [20] D. Li and T. Tang, “Stability analysis for the implicit-explicit discretization of the cahn-hilliard equation,” 08 2020.
- [21] D. Kay, V. Styles, and R. Welford, “Finite element approximation of a cahn-hilliard-navier-stokes system,” *Interfaces and Free Boundaries - INTERFACE FREE BOUND*, vol. 10, 01 2008.
- [22] G. Barros, A. Cortes, and A. Coutinho, *A Space-Time Adaptivity Scheme For The Cahn-Hilliard Equation*. PhD thesis, 03 2019.
- [23] Y. He, Y. Liu, and T. Tang, “On large time-stepping methods for the cahn–hilliard equation,” *Applied Numerical Mathematics*, vol. 57, no. 5, pp. 616–628, 2007. Special Issue for the International Conference on Scientific Computing.
- [24] J. Huang, H. Huang, and X. Wang, “Wetting boundary conditions in numerical simulation of binary fluids by using phase-field method: Some comparative studies and new development,” *International Journal for Numerical Methods in Fluids*, vol. 77, 11 2014.
- [25] E. Tadmor, “A review of numerical methods for nonlinear partial differential equations,” *Bulletin (New Series) of the American Mathematical Society*, vol. 49, 10 2012.
- [26] P. T. Boyanova, M. Do-Quang, and M. G. Neytcheva, “Solution methods for the cahn–hilliard equation discretized by conforming and non-conforming finite elements,” 2011.
- [27] X. Wu, “Preconditioners for the discrete cah-hilliard equation in three space dimensions,” 2011.
- [28] Y. Li, Y. Choi, and J. Kim, “Computationally efficient adaptive time step method for the cahn–hilliard equation,” *Computers & Mathematics with Applications*, vol. 73, no. 8, pp. 1855–1864, 2017.

## A The implementation

This chapter is devoted to the implementation aspects for the boundary value problems examined in the previous sections. The source code is written in FORTRAN, and it implements a backward Euler method with minor modifications, like convex splitting, or midpoint approximation of the chemical potential, and/or modifications on the standard Ginzburg-Landau potential for some runs. We opt for a fixed timepoint approach that has to be chosen accordingly to the remarks made for the stability/unique-solvability and convergence that are noted in the temporal discretization section of this work. For the better presentation of the implementation aspects, we consider two main programs named respectively: PERIODIC.f90 and CONTACTANGLE.f90 .

### A.1 Dependencies

The PERIODIC/CONTACTANGLE programs rely on the following dependencies:

- `iso_fortran_env`: Intrinsic module providing essential Fortran environment parameters.
- `BiCGStab_mod`: A custom module containing the BiCGStab solver implementation.
- `PARAMETERS_PERIODIC/CONTACTANGLE.inc`: An included configuration file that sets program parameters.

### A.2 Program Components

The PERIODIC/CONTACTANGLE programs consist of various components, including:

### A.3 Space and Time Coordinates

The program initializes space coordinates  $x$  and  $y$  for the simulation. These coordinates define the spatial domain over which the problem is solved. Additionally, it sets up time coordinates  $t$  to track the simulation's progression.

### A.4 Local to Global Node Numbering

The `nop` array represents local to global node connectivity list, allowing for the mapping of local node indices to global node indices. This mapping is crucial for assembling the system of equations.

### A.5 Order Parameter Variables

The program handles the order parameter, denoted as  $u$ , which corresponds to the Cahn-Hilliard equation's primary variable. It manages both `u_new` and `u_old` variables for tracking the solution's evolution over time.

### A.6 Chemical Potential Variables

An auxiliary variable, denoted as  $w$ , represents the chemical potential. Similar to the order parameter, it manages both `w_new` and `w_old` variables.

### A.7 Newton Tolerance Parameters

The program defines tolerance parameters for the Newton-Raphson method, including `tolS` for the convergence tolerance, `ntrial` for the maximum number of Newton iterations, and `max_iter` for the maximum number of iterations allowed in the BiCGStab solver.

## A.8 Stationary System of Newton Cycle

The `fvec` and `fjac` arrays represent the equation systems used in the Newton-Raphson iterations. These arrays contain the system's right-hand side (RHS) and the Jacobian matrix. To improve computational efficiency, the arrays are divided into four components: `fjac1`, `fjac2`, `fjac3`, and `fjac4`.

## A.9 Local Contributions

Local contributions from each element are accumulated into `fjac1`, `fjac2`, `fjac3`, and `fjac4`. Similarly, `fvec1` and `fvec2` store the local contributions to the right-hand side of the equation system.

## A.10 Newton Solution Vector

The `dSol` array represents the correction vector obtained from the Newton-Raphson iterations. It is added to the solution vector `Sol` to update the solution.

## A.11 Loop Variables

The program uses various loop variables, including `element`, `timepoint`, `trial`, `n`, `m`, and `L`. These variables control the program's flow and iteration.

## A.12 Convergence Check

A boolean variable, `CONVERGENT`, is used to check for convergence within the Newton-Raphson loop. The program stops iterating when convergence is achieved or after reaching the maximum number of iterations.

## A.13 File Handling

The program reads and writes data to files. The `OPEN`, `WRITE`, and `CLOSE` statements are used for file handling.

## A.14 Program Execution

The execution of the `PERIODIC/CONTACTANGLE` programs involves several steps:

1. Import the required dependencies, including `iso_fortran_env`, `BiCGStab_mod`, and `PARAMETERS_PERIODIC/CONTACTANGLE`.
2. Initialize space and time coordinates (`x`, `y`, and `t`).
3. Perform local-to-global node numbering (`nop`).
4. Set the initial conditions for the order parameter (`u_old` and `u_new`) and the chemical potential (`w_old` and `w_new`).
5. Enter a time loop to simulate the problem at various time points.
6. For each time point, perform a Newton-Raphson iteration to improve the solution.
7. Check for convergence within the Newton-Raphson loop.
8. Write results to output files at specified intervals.

## A.15 Space Discretization

```
SUBROUTINE SpaceDiscretization(x,y)
  use, intrinsic :: iso_fortran_env
  IMPLICIT NONE
  INCLUDE 'PARAMETERS_.inc'

  !> Space coordinates
  REAL(real64) x(NNmax),y(NNmax)

  REAL(real64) xorigin,yorigin,xlast,ylast
  REAL(real64) dx,dy
  INTEGER i,j,NNode

  x=0.0_real64
  y=0.0_real64

  xorigin=0.0_real64
  xlast=1.0_real64
  dx=(xlast-xorigin)/real(2*NELx)

  yorigin=0.0_real64
  ylast=1.0_real64
  dy=(ylast-yorigin)/real(2*NELy)

  !> Setting the coordinates of each node
  x(1)=xorigin
  y(1)=yorigin
  DO i=1,NNx
    NNode = (i-1)*NNy + 1 ! Ascending node numbering from bottom left up to right
    x(NNode) = x(1) + (i-1)*dx
    y(NNode) = y(1)
    DO j=2,NNy
      x(NNode+j-1)=x(NNode)
      y(NNode+j-1)=y(NNode)+(j-1)*dy
    ENDDO
  ENDDO
END SUBROUTINE SpaceDiscretization
```

## A.16 Global Node Numbering

```
SUBROUTINE GlobalNodeNumbering(nop)
  use, intrinsic :: iso_fortran_env
  IMPLICIT NONE
  INCLUDE 'PARAMETERS_.inc'

  !> Local to global space numbering
  INTEGER nop(NELmax,NNref)

  INTEGER i,j,k,l,NEL
  NEL=0
  DO i=1,NELx
    DO j=1,NELy
      NEL=NEL+1
      DO k=1,3
```

```

        l=3*k-2
        nop(nel,l)=nny*(2*i+k-3)+2*j-1
        nop(nel,l+1)=nop(nel,l)+1
        nop(nel,l+2)=nop(nel,l)+2
    ENDDO
ENDDO
END SUBROUTINE GlobalNodeNumbering

```

## A.17 Time Discretization

```

SUBROUTINE TimeDiscretization(t)
  use, intrinsic :: iso_fortran_env
  IMPLICIT NONE
  INCLUDE 'PARAMETERS_.inc'

  !> Time coordinates
  REAL(real64) t(Tmax)

  REAL(real64) Tinit

  INTEGER j

  Tinit=0.0_real64

  t(1)=Tinit
  DO j=2,Tmax
    t(j) = (j-1)*dt
  ENDDO

END SUBROUTINE TimeDiscretization

```

## A.18 Initial Conditions

```

SUBROUTINE InitialConditions(x, y, u_old,u_new,w_old,w_new)
  use, intrinsic :: iso_fortran_env
  IMPLICIT NONE
  INCLUDE 'PARAMETERS_.inc'

  !> Space coordinates
  REAL(real64), DIMENSION(NNmax) :: x, y

  !> Order parameter - c - of the Cahn Hilliard Equation
  REAL(real64), DIMENSION(NNmax) :: u_old
  REAL(real64), DIMENSION(NNmax) :: u_new

  !> Auxiliary variable - w - the chemical potential
  REAL(real64), DIMENSION(NNmax) :: w_old
  REAL(real64), DIMENSION(NNmax) :: w_new

  INTEGER :: i,n,m

```

```

DO i = 1, NNmax

    CALL RANDOM_NUMBER(u_old(i))
    !u_old(i) = 0.63_real64 + 0.02_real64*(0.5_real64-u_old(i))
    u_old(i) = 2.0_real64*u_old(i)-1.0_real64
    w_old(i) = 0.0_real64

ENDDO

```

```

END SUBROUTINE InitialConditions

```

## A.19 The system of each Newton cycle

This subroutine assembles the stationary system that is to be solved on every Newton iteration. Some different options for the potential and for the numerical scheme that are contained in comments, could be inserted in a parametric form in a more refined version of the code.

```

SUBROUTINE AssembleSystem(x,y,element,nop,u_old,u_new,w_new,w_old,fjac1,fjac2,fjac3,fjac4,fvec1,fvec2)
    use, intrinsic :: iso_fortran_env
    IMPLICIT NONE
    INCLUDE 'PARAMETERS_.inc'

    !> Space coordinates !xpt,ypt
    REAL(real64), INTENT(IN) :: x(NNmax),y(NNmax)

    !> Current element
    INTEGER element

    !> Local to global space numbering
    INTEGER nop(NELmax,NNref)
    INTEGER ngl(NNref)

    !> Order parameter - c - of the Cahn Hilliard Equation
    REAL(real64) u_new(NNmax)
    REAL(real64) u_old(NNmax)
    REAL(real64) w_new(NNmax)
    REAL(real64) w_old(NNmax)

    !> Local contributions
    REAL(real64) fjac1(NNmax,NNmax)
    REAL(real64) fjac2(NNmax,NNmax)
    REAL(real64) fjac3(NNmax,NNmax)
    REAL(real64) fjac4(NNmax,NNmax)

    REAL(real64) fvec1(NNmax)
    REAL(real64) fvec2(NNmax)

```



```

REAL(real64) phi(NNref), tphx(NNref), tphy(NNref), phic(NNref), phie(NNref)
REAL(real64) gp(3), gw(3)
REAL(real64) Xdomain, Xc, Xe, Ydomain, Yc, Ye, dett

REAL(real64) u0i, ui, ux, uy, wi, wx, w0x, wy, w0y
INTEGER i, r, k, l, m, n

gw = (/0.277777777777778, 0.444444444444444, 0.277777777777778/)
gp = (/0.1127016654      , 0.5                , 0.8872983346      /)

DO i = 1, NNref
  ngl(i) = nop(element, i)
ENDDO

! Loop over gauss points
DO r = 1, 3
  DO k = 1, 3

    call TestFunctions(gp(r), gp(k), phi, phic, phie)

    ! Defines the domain domain coordinates and the 2-dimensional Jacobian dett
    Xdomain=0.0_real64
    Xc=0.0_real64
    Xe=0.0_real64
    Ydomain=0.0_real64
    Yc=0.0_real64
    Ye=0.0_real64
    DO n=1, NNref
      Xdomain= Xdomain + x(ngl(n)) * phi(n)
      Xc= Xc + x(ngl(n)) * phic(n)
      Xe= Xe + x(ngl(n)) * phie(n)
      Ydomain= Ydomain + y(ngl(n)) * phi(n)
      Yc= Yc + y(ngl(n)) * phic(n)
      Ye= Ye + y(ngl(n)) * phie(n)
    ENDDO
    dett=Xc*Ye-Xe*Yc

    DO i=1, NNref
      tphx(i)=(Ye*phic(i)-Yc*phie(i))/dett
      tphy(i)=(Xc*phie(i)-Xe*phic(i))/dett
    ENDDO

    u0i = 0.0_real64
    ui = 0.0_real64
    ux = 0.0_real64
    uy = 0.0_real64
    wi = 0.0_real64
    wx = 0.0_real64
    w0x = 0.0_real64
    wy = 0.0_real64
  ENDO
ENDDO

```

```

w0y = 0.0_real64
DO i=1,NNref
  u0i = u0i + u_old(ngl(i))*phi(i)
  ui = ui + u_new(ngl(i))*phi(i)
  ux = ux + u_new(ngl(i))*tphx(i)
  uy = uy + u_new(ngl(i))*tphy(i)
ENDDO
DO i=1,NNref
  wi = wi + w_new(ngl(i))*phi(i)
  wx = wx + w_new(ngl(i))*tphx(i)
  w0x = w0x + w_old(ngl(i))*tphx(i)
  wy = wy + w_new(ngl(i))*tphy(i)
  w0y = w0y + w_old(ngl(i))*tphy(i)
ENDDO

!*****
!W = 100c**2(1-c)**2 FENICS
!*****
! DO l=1,NNref
!   f(ngl(l)) = f(ngl(l)) + gw(r)*gw(k)*dett*(100.0)*(ui**2)*(( 1.0 - ui)**2)*phi(l)
!   DO m=1,NNref
!     J(ngl(l),ngl(m)) = J(ngl(l),ngl(m)) + gw(r)*gw(k)*dett*(200.0)*(ui*(1.0-ui)*(1.0-2.0*
!   ENDDO
! ENDDO

!*****
!W = 0.25(c**2-1)**2 ginzburg landau
!*****
! DO l=1,NNref
!   f(ngl(l)) = f(ngl(l)) + gw(r)*gw(k)*dett*(ui**3 - ui)*phi(l)
!   DO m=1,NNref
!     J(ngl(l),ngl(m)) = J(ngl(l),ngl(m)) + gw(r)*gw(k)*dett*((3.0_real64)*(ui**2) - 1.0_rea
!   ENDDO
! ENDDO

!*****
!W = 0.25(c**2-1)**2 ginzburg landau & convex splitting
!*****
! DO l=1,NNref
!   f(ngl(l)) = f(ngl(l)) + gw(r)*gw(k)*dett*(ui**3)*phi(l)
!   DO m=1,NNref
!     J(ngl(l),ngl(m)) = J(ngl(l),ngl(m)) + gw(r)*gw(k)*dett*((3.0_real64)*(ui**2))*phi(l)*p
!   ENDDO
! ENDDO

DO l=1,NNref

fvec1(ngl(l)) = fvec1(ngl(l)) + gw(r)*gw(k)*dett*wi*phi(l) -gw(r)*gw(k)*dett*(100.0_real64)
-(e)**2*gw(r)*gw(k)*dett*(ux*tphx(l)+uy*tphy(l))

fvec2(ngl(l)) = fvec2(ngl(l)) + gw(r)*gw(k)*dett*ui*phi(l) - gw(r)*gw(k)*dett*u0i*phi(l) &
+ 0.5*(dt)*gw(r)*gw(k)*dett*(wx*tphx(l)+wy*tphy(l)) + 0.5*(dt)*gw(r)*gw(k)*dett*(w0x*tphx

```

```

DO m=1,NNref

    fjac1(ngl(1),ngl(m)) = fjac1(ngl(1),ngl(m)) + gw(r)*gw(k)*dett*phi(1)*phi(m)

    fjac2(ngl(1),ngl(m)) = fjac2(ngl(1),ngl(m)) - (e)**2*gw(r)*gw(k)*dett*(tphx(1)*tphx(m)+
    - gw(r)*gw(k)*dett*(100.0_real64)*((2.0_real64 - 12.0_real64*ui+ 12.0_real64*ui**2))*p

    fjac3(ngl(1),ngl(m)) = fjac3(ngl(1),ngl(m)) + (dt)*gw(r)*gw(k)*dett*(tphx(1)*tphx(m)+t

    fjac4(ngl(1),ngl(m)) = fjac4(ngl(1),ngl(m)) + gw(r)*gw(k)*dett*phi(1)*phi(m)

        ENDDO
    ENDDO
ENDDO
END SUBROUTINE AssembleSystem

```

## A.20 The test functions

```

SUBROUTINE TestFunctions(x,y,phi,phic,phie)
  use, intrinsic :: iso_fortran_env
  IMPLICIT NONE
  INCLUDE 'PARAMETERS_.inc'

  !> Point at which to form the test functions
  REAL(real64),DIMENSION(NNref):: phi,phic,phie
  REAL(real64), INTENT(IN) :: x,y
  REAL(real64) :: l1x, l2x, l3x, l1y, l2y, l3y
  REAL(real64) :: dl1x,dl2x,dl3x, dl1y, dl2y, dl3y

  !*** One Statement Functions !***
  l1x=2.*x**2-3.*x+1.
  l2x=-4.*x**2+4.*x
  l3x=2.*x**2-x
  dl1x=4.*x-3.
  dl2x=-8.*x+4.
  dl3x=4.*x-1.

  l1y=2.*y**2-3.*y+1.
  l2y=-4.*y**2+4.*y
  l3y=2.*y**2-y
  dl1y=4.*y-3.
  dl2y=-8.*y+4.
  dl3y=4.*y-1.
  !*****

  phi(1)=l1x*l1y
  phi(2)=l1x*l2y
  phi(3)=l1x*l3y
  phi(4)=l2x*l1y
  phi(5)=l2x*l2y

```

```

phi(6)=12x*13y
phi(7)=13x*11y
phi(8)=13x*12y
phi(9)=13x*13y
phic(1)=11y*d11x
phic(2)=12y*d11x
phic(3)=13y*d11x
phic(4)=11y*d12x
phic(5)=12y*d12x
phic(6)=13y*d12x
phic(7)=11y*d13x
phic(8)=12y*d13x
phic(9)=13y*d13x
phie(1)=11x*d11y
phie(2)=11x*d12y
phie(3)=11x*d13y
phie(4)=12x*d11y
phie(5)=12x*d12y
phie(6)=12x*d13y
phie(7)=13x*d11y
phie(8)=13x*d12y
phie(9)=13x*d13y

```

```
END SUBROUTINE TestFunctions
```

## B PERIODIC.f90

For the implementation of the periodic conditions we show only the essential modifications that the systems matrices/vectors undergo when we impose the conditions under the analysis stated in the relevant chapter of this work. After the system is assembled, the corresponding left-right and top-bottom node lines/rows of the system matrices are added, setting zero the residual on the right and top nodes and setting one to the systems Jacobian. Also a recovery of the boundary values for the right and top nodes follows after each iteration.

```

program PERIODIC
  use, intrinsic :: iso_fortran_env
  USE BiCGStab_mod
  IMPLICIT NONE
  INCLUDE 'PARAMETERS_PERIODIC.inc'

  !> Space coordinates
  REAL(real64) x(NNmax),y(NNmax)

  !> Time coordinates
  REAL(real64) t(Tmax)

  !> Local to global node numbering
  INTEGER nop(NELmax,NNref)

  !> Order parameter - u - of the Cahn Hilliard Equation
  REAL(real64) u_new(NNmax)
  REAL(real64) u_old(NNmax)

```

```

!> Auxiliary variable - w - the chemical potential
REAL(real64) w_new(NNmax)
REAL(real64) w_old(NNmax)

!> Newton tolerance parameters
REAL(real64),PARAMETER:: tolS=1.0E-5_real64
INTEGER, PARAMETER :: ntrial = 100
INTEGER, PARAMETER :: max_iter = 1000

!> Stationary system of Newton cycle
REAL(real64) fvec(2*NNmax)
REAL(real64) fjac(2*NNmax,2*NNmax)
!> Local contributions
REAL(real64) fjac1(NNmax,NNmax)
REAL(real64) fjac2(NNmax,NNmax)
REAL(real64) fjac3(NNmax,NNmax)
REAL(real64) fjac4(NNmax,NNmax)

REAL(real64) fvec1(NNmax)
REAL(real64) fvec2(NNmax)

!> Newton solution vector
REAL(real64) dSol(2*NNmax)
REAL(real64) Sol(2*NNmax)

INTEGER element,timepoint,trial,n,m,l
LOGICAL CONVERGENT
CHARACTER(10) :: timepoint_str

OPEN(unit=1,file='initial_PERIODIC.dat')

WRITE(*,'(25x,A)') 'Results c(n,t)'
CALL SpaceDiscretization(x,y)
CALL GlobalNodeNumbering(nop)

!> Set time grid
t=0.0_real64
CALL TimeDiscretization(t)

!>*****
!> Set the initial conditions for the c,w variables of the problem
!> For timepoint = 1
!>*****
u_old=0.0_real64
u_new=0.0_real64
w_old=0.0_real64
w_new=0.0_real64
CALL InitialConditions(x,y,u_old,u_new,w_old,w_new)

DO n=1,NNx

```

```

WRITE(1,*) (u_old((n-1)*NNy+m),m=1,NNy)
ENDDO
CLOSE(1)

```

```

!>*****
!> Given an initial guess x for a root in n dimensions, take ntrial Newton-Raphson
!> steps to improve the root. Stop if the root converges in either summed absolute
!> variable increments tolx or summed absolute function values tolf.
!>*****

```

```

!> Time loop to attain the solution at every timepoint

```

```

DO timepoint=2,Tmax
  print *, "Time point: ", timepoint

  trial=0
  CONVERGENT=.false.
  Sol=0.0_real64

```

```

!> Choose the initial guess for the first newton iteration
Sol(1:NNmax) = w_old(:)
Sol(NNmax+1:2*NNmax) = u_old(:)

```

```

!> Start the Newton iteration loop
DO WHILE (.NOT.CONVERGENT .AND. trial < ntrial)
  dSol=0.0_real64

```

```

!>*****
!> Set the Stationary System to be solved at every Newton iteration
!> _____Fjac.dx = -Fvec_____
!>*****
fvec=0.0_real64
fjac=0.0_real64

```

```

fjac1=0.0_real64
fjac2=0.0_real64
fjac3=0.0_real64
fjac4=0.0_real64

```

```

fvec1=0.0_real64
fvec2=0.0_real64

```

```

!> Local contributions

```

```

DO element=1,NELmax
CALL AssembleSystem(x,y,element,nop,u_old,u_new,w_new,fjac1,fjac2,fjac3,fjac4,fvec1,fvec2)
ENDDO

```

```

!> Global system
fvec(1:NNmax) = fvec1(:)
fvec(NNmax+1:2*NNmax) = fvec2(:)

```

```

fjac(1:NNmax,1:NNmax) = fjac1(:, :)

```

```

fjac(1:NNmax,NNmax+1:2*NNmax) = fjac2(:, :)
fjac(NNmax+1:2*NNmax,1:NNmax) = fjac3(:, :)
fjac(NNmax+1:2*NNmax,NNmax+1:2*NNmax) = fjac4(:, :)

!> Imposing the periodic conditions
DO l=1,NNy
  fvec(l) = fvec(l) + fvec(NNmax-NNy+1)
  fvec(NNmax-NNy+1) = 0.0_real64

  fjac(l,:) = fjac(l,:) + fjac(NNmax-NNy+1,:)
  fjac(:,l) = fjac(:,l) + fjac(:,NNmax-NNy+1)
  fjac(NNmax-NNy+1,:) = 0.0_real64
  fjac(:,NNmax-NNy+1) = 0.0_real64
  fjac(NNmax-NNy+1,NNmax-NNy+1) = 1.0_real64
ENDDO
DO l=2,NNx-1
  fvec((l-1)*NNy+1) = fvec((l-1)*NNy+1) + fvec(l*NNy)
  fvec(l*NNy) = 0.0_real64

  fjac((l-1)*NNy+1,:) = fjac((l-1)*NNy+1,:) + fjac(l*NNy,:)
  fjac(:,(l-1)*NNy+1) = fjac(:,(l-1)*NNy+1) + fjac(:,l*NNy)
  fjac(l*NNy,:) = 0.0_real64
  fjac(:,l*NNy) = 0.0_real64
  fjac(l*NNy,l*NNy) = 1.0_real64
ENDDO

!> Solve the system - find the correction dSol
fvec = -fvec
dSol = BiCGStab(fjac,fvec)

!> Recover the right boundary nodes
DO l=1,NNy
  dSol(NNmax-NNy+1) = dSol(1)
  dSol(2*NNmax-NNy+1) = dSol(NNmax+1)
ENDDO
!> Recover the top nodes
DO l=2,NNx-1
  dSol(l*NNy) = dSol((l-1)*NNy+1)
  dSol(NNmax+1*NNy) = dSol(NNmax+(l-1)*NNy+1)
ENDDO

!> Update the solution
Sol(:) = Sol(:) + dSol(:)

DO l=1,2*NNmax
  IF (Sol(l) <= - 0.9999) THEN
    Sol(l) = - 0.9999
  ELSEIF (Sol(l) >= 0.9999) THEN
    Sol(l) = 0.9999
  ENDIF
ENDDO

!> Check for convergence
CONVERGENT = (NORM2(dSol) < tolS)

```

```

    print*,"CONVERGENCE", CONVERGENT

    trial = trial + 1
    w_new(:) = Sol(1:NNmax)
    u_new(:) = Sol(NNmax+1:2*NNmax)

ENDDO  !> Newton trial loop

IF (CONVERGENT) THEN

    u_old(:) = u_new(:)
    w_old(:) = w_new(:)

    write(*,*) 'Newton-Raphson converged in', trial, 'iterations'

IF ((timepoint<=100 .and. MOD(timepoint,10)==0).or.MOD(timepoint, 500) == 0) THEN

    WRITE(timepoint_str, '(I0)') timepoint  ! Convert the integer to a string

    OPEN(UNIT=2, FILE=TRIM(ADJUSTL(timepoint_str)) // '_PERIODIC.dat')
    DO n = 1, NNx
        WRITE(2, *) (u_new((n - 1) * NNy + m), m = 1, NNy)
    ENDDO

    CLOSE(2)
ENDIF

ELSE
    write(*,*) 'Newton-Raphson did not converge within', ntrial, 'iterations'
ENDIF

ENDDO  !> Time loop

END program PERIODIC

```

## C CONTACTANGLE.f90

For the wetted wall conditions to be examined in this program the essential modifications concern the AssembleSystem subroutine, to take into account the wall energy term. For this purpose the first lines of this subroutine are modified to calculate the boundary integral term arising from the weak formulation.

```

SUBROUTINE AssembleSystem(x,y,element,BoundaryElement,BottomElement,RightElement,TopElement,LeftElement
    u_old,u_new,w_new,fjac1,fjac2,fjac3,fjac4,fvec1,fvec2,flux,dflux)
    use, intrinsic :: iso_fortran_env
    IMPLICIT NONE
    INCLUDE 'PARAMETERS_CONTACT.inc'

```

```

    !> Space coordinates !xpt,ypt

```



```

REAL(real64), INTENT(IN) :: x(NNmax),y(NNmax)

!> Current element
INTEGER element
!> Location indices to check for Boundary Elements
INTEGER BottomElement(NELmax)
INTEGER RightElement(NELmax)
INTEGER TopElement(NELmax)
INTEGER LeftElement(NELmax)

!> Boundary element control index
INTEGER BoundaryElement(NELmax)

!> Local to global space numbering
INTEGER nop(NELmax,NNref)
INTEGER ngl(NNref)

!> Order parameter - c - of the Cahn Hilliard Equation
REAL(real64) u_new(NNmax)
REAL(real64) u_old(NNmax)
REAL(real64) w_new(NNmax)

!> Local contributions
REAL(real64) fjac1(NNmax,NNmax)
REAL(real64) fjac2(NNmax,NNmax)
REAL(real64) fjac3(NNmax,NNmax)
REAL(real64) fjac4(NNmax,NNmax)

REAL(real64) fvec1(NNmax)
REAL(real64) fvec2(NNmax)

REAL(real64) flux(NNmax)
REAL(real64) fluxb(NNmax)
REAL(real64) fluxr(NNmax)
REAL(real64) fluxt(NNmax)
REAL(real64) fluxl(NNmax)

REAL(real64) Dflux(NNmax,NNmax)
REAL(real64) Dfluxb(NNmax,NNmax)
REAL(real64) Dfluxr(NNmax,NNmax)
REAL(real64) Dfluxt(NNmax,NNmax)
REAL(real64) Dfluxl(NNmax,NNmax)

REAL(real64) phi(NNref), tpx(NNref), tpy(NNref), phic(NNref), phie(NNref)
REAL(real64) gp(3), gw(3)
REAL(real64) Xdomain,Xc,Xe,Ydomain,Yc,Ye,dett

REAL(real64) u0i,ui,ux,uy,wi,wx,wy
INTEGER i,j,r,k,l,m,n

```

```

gw =(/0.277777777777778, 0.4444444444444, 0.27777777777778/)
gp =(/0.1127016654      , 0.5                , 0.8872983346      /)

DO i = 1,NNref
  ngl(i) = nop(element,i)
ENDDO

fluxb=0.0_real64
fluxr=0.0_real64
fluxt=0.0_real64
fluxl=0.0_real64

Dfluxb=0.0_real64
Dfluxr=0.0_real64
Dfluxt=0.0_real64
Dfluxl=0.0_real64

IF (BoundaryElement(element)==1) THEN

  !> check which side of the boundary the element belongs to
  IF (BottomElement(element)==1)THEN
    DO j=1,3
      CALL TestFunctions(gp(j),0.0_real64,phi, phic, phie)

      Xdomain=0.0_real64
      Xc=0.0_real64
      Xe=0.0_real64
      Ydomain=0.0_real64
      Yc=0.0_real64
      Ye=0.0_real64
      DO n=1,NNref
        Xdomain= Xdomain + x(ngl(n)) * phi(n)
        Xc= Xc + x(ngl(n)) * phic(n)
        Xe= Xe + x(ngl(n)) * phie(n)
        Ydomain= Ydomain + y(ngl(n)) * phi(n)
        Yc= Yc + y(ngl(n)) * phic(n)
        Ye= Ye + y(ngl(n)) * phie(n)
      ENDDO
      dett=Xc*Ye-Xe*Yc

      DO i=1,NNref
        tphx(i)=(Ye*phic(i)-Yc*phie(i))/dett
        tphy(i)=(Xc*phie(i)-Xe*phic(i))/dett
      ENDDO

      ui = 0.0_real64
      ux = 0.0_real64
      uy = 0.0_real64
      DO i=1,NNref
        ui = ui + u_new(ngl(i))*phi(i)
        ux = ux + u_new(ngl(i))*tphx(i)

```

```

    uy = uy + u_new(ngl(i))*tphy(i)
ENDDO

DO m=1,7,3
    fluxb(ngl(m)) = fluxb(ngl(m)) + gw(j)*dett*(1.0_real64-ui**2)*phi(m)
ENDDO

DO l=1,7,3
    DO m=1,7,3
        Dfluxb(ngl(l),ngl(m)) = Dfluxb(ngl(l),ngl(m)) +gw(j)*dett*(- 2.0_real64*ui*phi(m))*ph
    ENDDO
ENDDO
ENDDO

IF (RightElement(element)==1)THEN
DO j=1,3
    CALL TestFunctions(1.0_real64,gp(j),phi, phic, phie)

    Xdomain=0.0_real64
    Xc=0.0_real64
    Xe=0.0_real64
    Ydomain=0.0_real64
    Yc=0.0_real64
    Ye=0.0_real64
    DO n=1,NNref
        Xdomain= Xdomain + x(ngl(n)) * phi(n)
        Xc= Xc + x(ngl(n)) * phic(n)
        Xe= Xe + x(ngl(n)) * phie(n)
        Ydomain= Ydomain + y(ngl(n)) * phi(n)
        Yc= Yc + y(ngl(n)) * phic(n)
        Ye= Ye + y(ngl(n)) * phie(n)
    ENDDO
    dett=Xc*Ye-Xe*Yc

    DO i=1,NNref
        tphx(i)=(Ye*phic(i)-Yc*phie(i))/dett
        tphy(i)=(Xc*phie(i)-Xe*phic(i))/dett
    ENDDO

    ui = 0.0_real64
    ux = 0.0_real64
    uy = 0.0_real64
    DO i=1,NNref
        ui = ui + u_new(ngl(i))*phi(i)
        ux = ux + u_new(ngl(i))*tphx(i)
        uy = uy + u_new(ngl(i))*tphy(i)
    ENDDO

DO m=7,9
    fluxr(ngl(m)) = fluxr(ngl(m)) +gw(j)*dett*(1.0_real64-ui**2)*phi(m)
ENDDO

```

```

DO l=7,9
  DO m=7,9
    Dfluxr(ngl(1),ngl(m)) = Dfluxr(ngl(1),ngl(m)) + gw(j)*dett*(- 2.0_real64*ui*phi(m))*p
  ENDDO
ENDDO
ENDDO

ELSEIF (TopElement(element)==1)THEN
DO j=1,3
  CALL TestFunctions(gp(j),1.0_real64,phi, phic, phie)

  Xdomain=0.0_real64
  Xc=0.0_real64
  Xe=0.0_real64
  Ydomain=0.0_real64
  Yc=0.0_real64
  Ye=0.0_real64
  DO n=1,NNref
    Xdomain= Xdomain + x(ngl(n)) * phi(n)
    Xc= Xc + x(ngl(n)) * phic(n)
    Xe= Xe + x(ngl(n)) * phie(n)
    Ydomain= Ydomain + y(ngl(n)) * phi(n)
    Yc= Yc + y(ngl(n)) * phic(n)
    Ye= Ye + y(ngl(n)) * phie(n)
  ENDDO
  dett=Xc*Ye-Xe*Yc

  DO i=1,NNref
    tphx(i)=(Ye*phic(i)-Yc*phie(i))/dett
    tphy(i)=(Xc*phie(i)-Xe*phic(i))/dett
  ENDDO

  ui = 0.0_real64
  ux = 0.0_real64
  uy = 0.0_real64
  DO i=1,NNref
    ui = ui + u_new(ngl(i))*phi(i)
    ux = ux + u_new(ngl(i))*tphx(i)
    uy = uy + u_new(ngl(i))*tphy(i)
  ENDDO

  DO m=3,9,3
    fluxt(ngl(m)) = fluxt(ngl(m)) + gw(j)*dett*(1.0_real64-ui**2)*phi(m)
  ENDDO

  DO l=3,9,3
    DO m=3,9,3
      Dfluxt(ngl(1),ngl(m)) = Dfluxt(ngl(1),ngl(m)) + gw(j)*dett*(- 2.0_real64*ui*phi(m))*p
    ENDDO
  ENDDO
ENDDO

ELSEIF (LeftElement(element)==1)THEN

```

```

DO j=1,3
  CALL TestFunctions(0.0_real64,gp(j),phi, phic, phie)

  Xdomain=0.0_real64
  Xc=0.0_real64
  Xe=0.0_real64
  Ydomain=0.0_real64
  Yc=0.0_real64
  Ye=0.0_real64
  DO n=1,NNref
    Xdomain= Xdomain + x(ngl(n)) * phi(n)
    Xc= Xc + x(ngl(n)) * phic(n)
    Xe= Xe + x(ngl(n)) * phie(n)
    Ydomain= Ydomain + y(ngl(n)) * phi(n)
    Yc= Yc + y(ngl(n)) * phic(n)
    Ye= Ye + y(ngl(n)) * phie(n)
  ENDDO
  dett=Xc*Ye-Xe*Yc

  DO i=1,NNref
    tphx(i)=(Ye*phic(i)-Yc*phie(i))/dett
    tphy(i)=(Xc*phie(i)-Xe*phic(i))/dett
  ENDDO

  ui = 0.0_real64
  ux = 0.0_real64
  uy = 0.0_real64
  DO i=1,NNref
    ui = ui + u_new(ngl(i))*phi(i)
    ux = ux + u_new(ngl(i))*tphx(i)
    uy = uy + u_new(ngl(i))*tphy(i)
  ENDDO

  DO m=1,3
    fluxl(ngl(m)) = fluxl(ngl(m)) + gw(j)*dett*(1.0_real64-ui**2)*phi(m)
  ENDDO

  DO l=1,3
    DO m=1,3
      Dfluxl(ngl(l),ngl(m)) = Dfluxl(ngl(l),ngl(m)) + gw(j)*dett*(- 2.0_real64*ui*phi(m))*p
    ENDDO
  ENDDO
ENDDO

ENDIF
ENDIF

!> Summation of the components to the total FLUX
DO l=1,NNref
  flux(ngl(l)) = fluxb(ngl(l)) + fluxr(ngl(l)) + fluxt(ngl(l)) + fluxl(ngl(l))
  DO m=1,NNref
    Dflux(ngl(l),ngl(m)) = Dflux(ngl(l),ngl(m)) &

```

```

        + Dfluxb(ngl(1),ngl(m)) + Dfluxr(ngl(1),ngl(m)) + Dfluxt(ngl(1),ngl(m)) + Dfluxl(ngl(1),ngl(m))
    ENDDO
ENDDO
! Loop over gauss points

ENDIF

! Loop over gauss points
DO r = 1,3
    DO k = 1,3

        call TestFunctions(gp(r),gp(k),phi,phic,phie)

        ! Defines the domain domain coordinates and the 2-dimensional Jacobian dett
        Xdomain=0.0_real64
        Xc=0.0_real64
        Xe=0.0_real64
        Ydomain=0.0_real64
        Yc=0.0_real64
        Ye=0.0_real64
        DO n=1,NNref
            Xdomain= Xdomain + x(ngl(n)) * phi(n)
            Xc= Xc + x(ngl(n)) * phic(n)
            Xe= Xe + x(ngl(n)) * phie(n)
            Ydomain= Ydomain + y(ngl(n)) * phi(n)
            Yc= Yc + y(ngl(n)) * phic(n)
            Ye= Ye + y(ngl(n)) * phie(n)
        ENDDO
        dett=Xc*Ye-Xe*Yc

        DO i=1,NNref
            tphx(i)=(Ye*phic(i)-Yc*phie(i))/dett
            tphy(i)=(Xc*phie(i)-Xe*phic(i))/dett
        ENDDO

        u0i = 0.0_real64
        ui = 0.0_real64
        ux = 0.0_real64
        uy = 0.0_real64
        wi = 0.0_real64
        wx = 0.0_real64
        wy = 0.0_real64
        DO i=1,NNref
            u0i = u0i + u_old(ngl(i))*phi(i)
            ui = ui + u_new(ngl(i))*phi(i)
            ux = ux + u_new(ngl(i))*tphx(i)
            uy = uy + u_new(ngl(i))*tphy(i)
        ENDDO
        DO i=1,NNref
            wi = wi + w_new(ngl(i))*phi(i)
            wx = wx + w_new(ngl(i))*tphx(i)
            wy = wy + w_new(ngl(i))*tphy(i)
        ENDDO
    ENDDO
ENDDO

```

```

!*****
!W = 100c**2(1-c)**2 FENICS
!*****
! DO l=1,NNref
!   f(ngl(1)) = f(ngl(1)) + gw(r)*gw(k)*dett*(100.0)*(ui**2)*(( 1.0 - ui)**2)*phi(1)
!     DO m=1,NNref
!       J(ngl(1),ngl(m)) = J(ngl(1),ngl(m)) + gw(r)*gw(k)*dett*(200.0)*(ui*(1.0-ui)*(1.0-2.0*
!     ENDDO
! ENDDO

!*****
!W = 0.25(c**2-1)**2 ginzburg landau
!*****
! DO l=1,NNref
!   f(ngl(1)) = f(ngl(1)) + gw(r)*gw(k)*dett*(ui**3 - ui)*phi(1)
!     DO m=1,NNref
!       J(ngl(1),ngl(m)) = J(ngl(1),ngl(m)) + gw(r)*gw(k)*dett*((3.0_real64)*(ui**2) - 1.0_real64)
!     ENDDO
! ENDDO

!*****
!W = 0.25(c**2-1)**2 ginzburg landau & convex splitting
!*****
! DO l=1,NNref
!   f(ngl(1)) = f(ngl(1)) + gw(r)*gw(k)*dett*(ui**3)*phi(1)
!     DO m=1,NNref
!       J(ngl(1),ngl(m)) = J(ngl(1),ngl(m)) + gw(r)*gw(k)*dett*((3.0_real64)*(ui**2))*phi(1)+
!     ENDDO
! ENDDO

DO l=1,NNref

fvec1(ngl(1)) = fvec1(ngl(1)) + gw(r)*gw(k)*dett*wi*phi(1) - (1.0_real64/e)*gw(r)*gw(k)*dett*
- (e)*gw(r)*gw(k)*dett*(ux*tphx(1)+uy*tphy(1)) + (sqrt(2.0_real64)/2.0_real64)*cos(theta)*fl

fvec2(ngl(1)) = fvec2(ngl(1)) + gw(r)*gw(k)*dett*ui*phi(1) - gw(r)*gw(k)*dett*u0i*phi(1)
+ (dt)*gw(r)*gw(k)*dett*(wx*tphx(1)+wy*tphy(1))

DO m=1,NNref

fjac1(ngl(1),ngl(m)) = fjac1(ngl(1),ngl(m)) + gw(r)*gw(k)*dett*phi(1)*phi(m)

fjac2(ngl(1),ngl(m)) = fjac2(ngl(1),ngl(m)) - (e)*gw(r)*gw(k)*dett*(tphx(1)*tphx(m)+tph
- (1.0_real64/e)* gw(r)*gw(k)*dett*((3.0_real64)*(ui**2) - 1.0_real64)*phi(1)*phi(m) +

fjac3(ngl(1),ngl(m)) = fjac3(ngl(1),ngl(m)) + (dt)*gw(r)*gw(k)*dett*(tphx(1)*tphx(m)+

fjac4(ngl(1),ngl(m)) = fjac4(ngl(1),ngl(m)) + gw(r)*gw(k)*dett*phi(1)*phi(m)

ENDDO
ENDDO
ENDDO
ENDDO

```

END SUBROUTINE AssembleSystem